Journal of the European Meteorological Society 2 (2025) 100007

Contents lists available at ScienceDirect

Journal of the European Meteorological Society

journal homepage: https://www.sciencedirect.com/journal/journal-of-the-european-meteorological-society

The Land Surface Interactions with the Atmosphere over the Iberian Semi-Arid Environment (LIAISE) field campaign

Aaron Boone [a,*], Joaquim Bellvert [b], Martin Best [c], Jennifer K. Brooke [c], Guylaine Canut-Rocafort [a], Joan Cuxart [d], Oscar Hartogensis [e], Patrick Le Moigne [a], Josep Ramon Miró [f], Jan Polcher [h], Jeremy Price [c], Pere Quintana Seguí [g], Joan Bech [m,w], Yannick Bezombes [j], Oliver Branch [p], Jordi Cristóbal [r], Karin Dassas [i], Pascal Fanise [i], Fabien Gibert [h], Yves Goulas [h], Jannis Groh [t,u,v], Jan Hanus [l], Gabriel Hmimina [h], Lionel Jarlan [i], Ed Kim [q], Valérie Le Dantec [i], Michel Le Page [i], Fabienne Lohou [j], Marie Lothon [j], Mary Rose Mangan [e], Belén Martí [a,d], Daniel Martínez-Villagrasa [d], James McGregor [c], Amanda Kerr-Munslow [c], Nadia Ouaadi [i,n], Alban Philibert [j,s], Juan Quiros-Vargas [k], Uwe Rascher [k], Bastian Siegmann [k], Mireia Udina [m], Antoine Vial [j], Burkhard Wrenger [o], Volker Wulfmeyer [p], Mehrez Zribi [i]

[a] CNRM-Université de Toulouse, Météo-France/CNRS, 42 ave. G. Coriolis, 31057, Toulouse, France
[b] Efficient Use of Water in Agriculture Program, IRTA, Parc Agrobiotech Lleida Parc de Gardeny, Edifici Fruitcentre 25003, Lleida, Spain
[c] UKMO, FitzRoy Road, Exeter Devon EX1 3PB, United Kingdom
[d] Department of Physics, University of the Balearic Islands, Cra. de Valldemossa, km 7,5. 07122 Palma, Majorca, Spain
[e] Wageningen University, Meteorology and Air Quality Group, Droevendaalsesteeg 3, 6708 PB, Wageningen, The Netherlands
[f] Servei Meteorològic de Catalunya, C/Berlín núm. 38-48 4a, 08029, Barcelona, Spain
[g] Observatori de l'Ebre, Universitat Ramon Llull-CSIC, Carrer Observatori 3-A. 43520 Roquetes, Spain
[h] Laboratoire de Météorologie Dynamique (LMD/IPSL), École Polytechnique, Institut Polytechnique de Paris, ENS, PSL Research University, Sorbonne Université, CNRS, F91128 Palaiseau, France
[i] CESBIO, UMR 5126 Université Toulouse UT3/CNRS/IRD/CNES et USC INRAe, 18 av. Edouard Belin, bpi 2801, 31401 Toulouse cedex 9, France
[j] Laboratoire d'Aérologie, Université de Toulouse, CNRS, UPS, 14 avenue Edouard Belin 31400, Toulouse, France
[k] Institute of Bio and Geosciences, IBG-2: Plant Sciences, Forschungszentrum Jülich GmbH, 52428 Jülich, Germany
[l] Global Change Research Institute of the Czech Academy of Sciences - CzechGlobe, Bělidla 986/4a, 603 00 Brno-střed, Czech Republic
[m] Department of Applied Physics, University of Barcelona, C/Martí i Franquès, 1, 08028, Barcelona, Spain
[n] Centre for Remote Sens. Applications (CRSA), Mohammed VI Polytechnic University (UM6P), Lot 660, Hay Moulay Rachid, 43150, Ben Guerir, Morocco
[o] Ostwestfalen-Lippe University of Applied Sciences and Arts, Department of Environmental Engineering and Computer Sciences, An d. Wilhelmshöhe 44, 37671, Höxter, Germany
[p] Inst. for Physics and Meteorology, University of Hohenheim, Garbenstraße 30, 70599, Stuttgart, Germany
[q] NASA Goddard Space Flight Center, 8800 Greenbelt Rd, Greenbelt, MD 20771, USA
[r] Department of Geography. Universitat Autònoma de Barcelona, Campus de Bellaterra, Edifici B, Carrer de la Fortuna, s/n, 08193 Bellaterra, Spain
[s] Institut de Recherche en Astrophysique et Planétologie, Université de Toulouse, CNRS, UPS, 14 Avenue Édouard Belin - OMP 31400, France
[t] University of Bonn, Institute of Crop Science and Resource Conservation (INRES) – Soil Science and Soil Ecology, Nußallee 13, 53115, Bonn, Germany
[u] Leibniz Centre for Agricultural Landscape Research (ZALF), Research Area 1 "Landscape Functioning", Working group "Isotope Biogeochemistry and Gas Fluxes", Eberswalder Str. 84, 15374, Müncheberg, Germany
[v] Institute of Bio and Geosciences, IBG-3: Agrosphere, Forschungszentrum Jülich GmbH, 52428 Jülich, Germany
[w] Water Research Institute, University of Barcelona, C/Martí i Franqués, 1, 08028, Barcelona, Spain

ARTICLE INFO

Keywords:
Anthropization
Irrigation
Agriculture
Field campaign
Surface energy budget

ABSTRACT

One of the greatest challenges facing environmental science is to better understand the impacts of predicted future changes in the terrestrial hydrological cycle. It has been recognized that human activities play a key role and must therefore be considered in future climate simulations. The representation of anthropization in land surface schemes within global earth system models is at a relatively nascent stage and must be improved for more accurate future projections of water resources. The understanding of the impact of anthropogenic

* Correspondence to: CNRM/GMME/SURFACE, Météo-France, 42 avenue Gustave Coriolis, 31057, Toulouse cedex, France.
E-mail address: aaron.boone@meteo.fr (A. Boone).

https://doi.org/10.1016/j.jemets.2025.100007
Received 24 June 2024; Received in revised form 2 December 2024; Accepted 4 January 2025
Available online 18 January 2025

Evapotranspiration
Land–atmosphere interactions
Ebro basin

processes has been hampered by the lack of consistent and extensive observations. Here, we present the Land surface Interactions with the Atmosphere over the Iberian Semi-arid Environment (LIAISE) project field campaign which brought together ground-based (surface energy budget estimated at 7 sites, 269 radio soundings made at 2 sites and multiple remote sensing instruments for profiling the lower atmosphere), airborne measurements (3 airplanes and numerous drones measuring surface and atmospheric properties) and satellite data (to derive estimates of irrigation timing, soil moisture, evapotranspiration and surface temperature) to improve our understanding of key natural and anthropogenic land processes and boundary layer feedbacks. The study area is in the Ebro basin of northeastern Spain in a hot, dry Mediterranean climate, with a sharp demarcation between a vast intensively irrigated region and a much drier rainfed zone to the east. Analysis of the observations reveal strong surface heterogeneities of evapotranspiration within the irrigated zone (differences upwards of approximately 7 mm day-1 between fields), linked to the crop type, vegetation phenology and soil moisture, all of which were modulated by irrigation. The significant surface flux differences between the irrigated and rainfed zones were found to result in strongly contrasting atmospheric boundary layer properties (between 2 supersites separated by 14 km) extending upwards through the lowest several km of the atmosphere.

1. Introduction

One of the greatest challenges facing environmental science is understanding future changes in the terrestrial hydrological cycle and their resulting impacts on water resources. International organizations, such as the World Climate Research Programme (WCRP), have recognized that human activities play a key role in modifying the continental water cycle and must therefore be considered in climate change projections and water resource impact studies. This issue is particularly critical for agricultural areas in regions where water resources are already limited, such as the Mediterranean basin. Climate projections from the Coupled Model Intercomparison Project Phase 5 (CMIP5: Taylor et al., 2012) predict that the Mediterranean region will be a climate change "hot spot" in the twenty-first century (Diffenbaugh and Giorgi, 2012), characterized by greater interannual precipitation variability, more frequent heat waves, and overall warming and drying trends. More recently, Cos et al. (2022) analyzed CMIP6 (Eyring et al., 2016) simulations and showed that the predicted future warming and drying in the Mediterranean region are more related to global than regional trends. Nevertheless, the Iberian Peninsula is expected to experience increasing stress on water resources due to warmer and drier conditions projected for the twenty-first century. With rainfall largely confined to the autumn and spring seasons, human management of natural river systems is required to provide water for crops, as well as for a growing population and expanding agricultural activities. This includes the irrigation of crops that have historically received little or no irrigation, such as wine grapes (van Leeuwen et al., 2024), along with olives and almonds. These considerations highlight the need for well-managed irrigation to maintain sustainable agriculture in the future (Pörtner et al., 2022).

Irrigation is known to have a significant impact on the partitioning of latent and sensible heat fluxes in the surface energy budget (SEB), and thus on near-surface atmospheric state variables (e.g., Jiang et al. 2014; Phillips et al., 2022). Consequently, irrigation can potentially affect local atmospheric boundary layer (ABL) properties, thereby altering near-surface atmospheric conditions within and downwind of irrigated areas (e.g., Lawston et al., 2020), mesoscale circulation patterns (e.g., Mahrt et al., 1994; Lunel et al., 2024a), and potentially the regional-scale recycling of precipitation (Lo and Famiglietti, 2013; Alter et al., 2015; Udina et al., 2024). Brooke et al. (2023) showed that contrasts in near-surface meteorological parameters and boundary-layer thermodynamic profiles are established during the morning transition, developing rapidly shortly after sunrise, and becoming well established by convective onset. Cuxart et al. (2012) provided observational evidence of an enhanced nocturnal jet during summer over the Ebro basin, attributed to stronger nighttime thermal contrasts between irrigated zones and higher surrounding slopes. In addition, irrigated zones often contain reservoirs, which can further enhance regional or mesoscale evapotranspiration (ET). Reservoirs, as areas of potentially large evaporation rates, are also likely to impact the ABL. While it is generally accepted that the magnitude of irrigation's impact on the atmosphere depends on geographic location and climate, there remains debate over whether its effects are primarily local or can extend to larger scales, influencing regional circulation and precipitation patterns (Lo and Famiglietti, 2013).

The representation of the surface energy budget (SEB), particularly the ability to model radiative and turbulent interactions between the canopy airspace and the ground, is crucial for simulating surface fluxes over sparse or heterogeneous vegetation. However, it is well known that climate predictions over semi-arid regions are prone to biases in climate model variables, especially land surface temperature (LST), soil moisture, surface runoff, and SEB components, which can in turn affect land–atmosphere coupling and feedback mechanisms. This issue is exacerbated by the Mediterranean basin's highly heterogeneous land cover, characterized by a mix of natural and anthropized surfaces. The current representation of anthropization in land surface models (LSMs), and consequently in global climate models (GCMs), is at a relatively early stage and requires urgent improvement to produce accurate future projections of water resources and changes in the global water cycle (Harding et al., 2015). A key challenge is improving the estimation of evapotranspiration (ET) from semi-arid natural and anthropized surfaces, including irrigated and non-irrigated crops, for both practical applications and modeling studies. The eddy correlation technique is the most widely used method to estimate the turbulent flux components of the SEB (Cuxart and Boone, 2020). These flux estimates can be compared with ET measurements obtained from weighable lysimeters (Hirschi et al., 2017), facilitating comparisons between irrigation demand as simulated by LSMs and actual irrigation practices in the region. A critical consideration is obtaining quantitative estimates of the partitioning among different ET components, particularly since bare soil evaporation typically represents a "water loss" (i.e., a reduction in water use efficiency) in irrigated areas (Agam et al., 2012). This partitioning can be assessed for crops using eddy covariance techniques combined with isotopic analyses (e.g., Aouade et al., 2016; Quade et al., 2019), sap-flow measurements (Cammalleri et al., 2013), and weighing lysimeters (Rafi et al., 2019).

The understanding of the impact of anthropogenic processes in Earth system models has been hindered by a lack of consistent and extensive observations. Numerous field campaigns have focused on water resource issues in semi-arid landscapes across different regions of the world. Examples include the European Field Experiment in a Desertification-Threatened Area (EFEDA: Bolle, 1995), the Hydrologic Atmospheric Pilot Experiment in the Sahel (HAPEX-Sahel: Goutorbe et al., 1997), the Semi-Arid Land–Surface–Atmosphere (SALSA) program (Goodrich et al., 2000), and the Grape Remote Sensing Atmospheric Profile and Evapotranspiration Experiment (GRAPEX: Kustas et al., 2018). The Bushland Evapotranspiration and Agricultural Remote Sensing Experiment of 2008 (BEAREX08) (Evett et al., 2012) was conducted to improve the understanding of evaporative water use and efficiency in semi-arid irrigated areas. In particular, it examined the impact of mesoscale advection from arid regions on irrigated

fields and its influence on locally measured evapotranspiration (ET). In recent years, advances in land surface and atmospheric observing capabilities, coupled with the expansion of irrigated areas, have created renewed opportunities for dedicated field campaigns in contrasting climatic regions. For example, the Great Plains Irrigation Experiment (GRAINEX), conducted in summer 2018, investigated the effects of irrigation on coupled surface-atmosphere processes over a mesoscale region in eastern Nebraska (Rappin et al., 2021).

Here, we present an overview of the Land Surface Interactions with the Atmosphere over the Iberian Semi-Arid Environment (LIAISE) project, initiated under the auspices of the Hydrological Cycle in the Mediterranean Experiment (HyMeX: Drobinski et al., 2014) project. The overarching objective of LIAISE is to enhance our understanding of the impact of anthropization on the water cycle, focusing on land–atmosphere–hydrology interactions and the limitations of models in representing all aspects of the terrestrial water cycle in the semi-arid environment of the Iberian Peninsula. The key topics addressed by LIAISE include: (i) the influence of heterogeneity in land cover, including large irrigated areas, on area-averaged surface fluxes of momentum, heat, and moisture, (ii) the consequences of land–atmosphere interactions on local precipitation initiation and boundary layer evolution, (iii) the interactions between soil moisture and the atmosphere, (iv) the interactions among soil moisture, reservoirs, and groundwater in both natural and irrigated regions, (v) the impact of anthropogenic changes on runoff generation and its influence on streamflow and reservoir storage, and (vi) the implications of human activities for the future evolution of the hydrological cycle. The acronym LIAISE was chosen deliberately, as the English word "liaise" signifies cooperation on a matter of mutual concern, aptly reflecting the project's goal of achieving a better understanding of the impact of anthropization on the regional water cycle.

The LIAISE study area is situated in the Ebro Basin of northeastern Spain, within the Urgell region. This region has a semi-arid, hot, and dry Mediterranean climate, with a sharp demarcation between an almost continuously irrigated area and the much drier rainfed zone to the east of the study area. Water for this region is supplied by the 150-year-old Urgell Canal, which originates in the Pyrénées mountains to the north and supports several irrigation districts. In 2021, the canal irrigated a surface area of approximately 90,000 hectares (Bellvert et al., 2024). Most agricultural fields in the Urgell region utilize traditional flood (or gravity) irrigation, which is employed for orchards (mainly apple and pear), annual crops such as maize, and semi-perennial crops like alfalfa. Water delivery turns occur on average every 10 days. During each turn, leveled fields (designed to minimize the effects of local slopes) are inundated from a single distribution point. Sprinkler systems, including pivots and ramps, have been installed and are primarily used for crops such as barley and maize. Similarly, a small proportion of plots are equipped with drip irrigation systems, which are mainly used for high-value "cash crops" like broccoli and certain fruit orchards. Despite these advancements, fields utilizing sprinkler and drip irrigation systems still constitute only a small fraction of the total irrigated area.

This paper presents a summary of the intensive phase of the LIAISE field campaign, which brought together ground-based and airborne measurements, satellite data, and modeling studies to improve our understanding of key natural and anthropogenic land processes and their subsequent feedbacks with the Mediterranean boundary layer and the basin-scale hydrological cycle. These observations provide data that highlight gaps in our knowledge and identify current model deficiencies in land surface processes and land–atmosphere interactions within a semi-arid region characterized by strong surface heterogeneity due to contrasts between the natural landscape and intensive agriculture. A summary of the 2021 field campaign measurements is provided in Section 2. Several products derived from the field data are summarized in Section 3, and the conclusions along with some perspectives are discussed in Section 4.

2. LIAISE field campaign

The LIAISE study area is located in the Ebro Basin in northeastern Spain, bounded by the Pyrenees to the north and the Iberian System to the south. Surface heterogeneity in this region has increased due to human activity, which has significantly modified the hydrological cycle and landscape, primarily through intensive agricultural practices. Most of the basin's runoff is generated in the Pyrenees, prompting the construction of infrastructure to store and transport water from the mountainous areas to agricultural fields. Approximately 75% of the water used for agriculture is stored in reservoirs, while the remainder relies on the snowpack in the mountains. This infrastructure has boosted agricultural production and greatly expanded irrigated areas. However, it has also led to the abandonment of agricultural lands in the headwaters region, resulting in forest expansion, increased evapotranspiration (ET), and reduced river flows. Consequently, the human component of the Ebro system cannot be excluded from any study seeking to understand the basin's water cycle, which is influenced by both meteorological and hydrological processes.

The field campaign focused on an approximately 30 × 30 km area located in the eastern part of the basin, covering the Catalan counties of Urgell and Pla d'Urgell (Fig. 1). In this figure, the Normalized Difference Vegetation Index (NDVI) for June 24, 2021, is shown. The deeper green shades correspond to denser vegetation coverage within the irrigated zone on the plain, as well as in forested areas at higher altitudes to the east-southeast and north of the irrigated zone. The locations of the seven sites with surface measurements (described in Section 2.7) are indicated by triangles. Within the study area, the Canal d'Urgell runs roughly north–south, separating the two zones and providing irrigation water primarily to the west. The principal source of water for this canal is reservoirs in the upper Segre basin in the Pre-Pyrenees, to the north of the study area (Vicente-Serrano et al., 2017). Most of the irrigation in the LIAISE study area is flood irrigation, although some areas in the eastern part of the region use drip irrigation, fed by the Segarra-Garrigues canal (Ricart et al., 2016).

2.1. Observing period strategy

The main goal of the campaign was to acquire data that would improve the understanding of land–surface–atmosphere interactions over two contrasting areas (with and without irrigation) and how such contrasts potentially impact atmospheric circulation over this region. LIAISE uses a multidisciplinary approach, consisting of a suite of land surface models (LSMs) and hydrological and meteorological models that employ remote sensing data or data assimilation strategies to prescribe input parameters and perform evaluations. The observational strategy consisted of three periods in 2021:

1. The Long Observation Period (LOP) monitored slowly evolving land surface state variables (such as soil moisture, evapotranspiration (ET), and soil temperature) and relatively autonomous surface flux measurements at five sites, each characterized by different but regionally representative land cover types. This period covered the growing season of summer crops, ending in October or November. Standard meteorological variables were also measured.
2. The Special Observation Period (SOP) took place from July 15–29, when contrasts between irrigated and natural surfaces were generally at or near their maximum. Intensive ground-based and airborne measurements of the atmospheric boundary layer (ABL) were conducted, along with ecophysiological observations and high-spatial-resolution mesoscale remote sensing of surface variables from aircraft and unmanned aerial vehicles (UAVs). Two additional local-scale energy budgets and soil moisture sites were added for the SOP to calibrate or evaluate surface remote sensing data from aircraft.

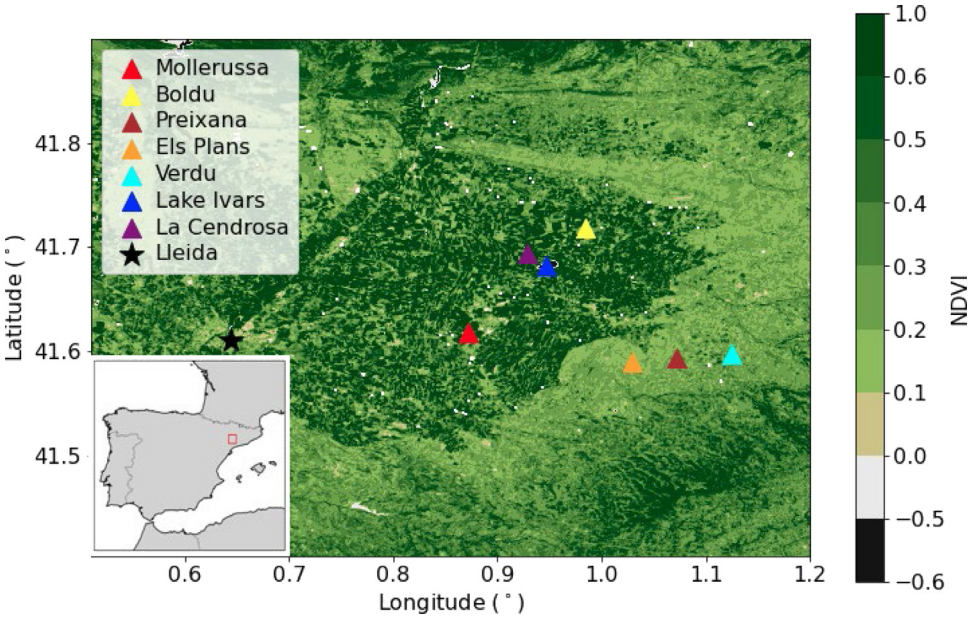

Fig. 1. The NDVI on the 24th of June 2021, shown over the LIAISE region. The location over Catalonia is shown in the lower left inset. The corresponding type of land cover for each of the test sites can be found in Table 3. The observation sites are indicated by symbols, and they are described in Section 2.7. The location of Lleida (not an observation site) is included for reference. Negative values indicate missing or flagged data. The NDVI data is the Copernicus Sentinel-2 (processed by ESA), 2021, MSI Level-2 A BOA Reflectance Product, Collection 0, (doi.org/10.5270/S2_-6eb6imz) from the European Space Agency.

3. The Intensive Observation Periods (IOPs) were defined as days within the SOP that had sufficiently good meteorological conditions to justify the full complement of measurements described in point 2. Fortuitously, the weather during the SOP was nearly ideal, allowing for 11 IOP days.

2.1.1. Salient weather conditions

In late July, synoptic-scale winds are typically light and come from the west, and a thermal (heat) low generally forms over the region, with daily highs in the mid to upper 30s°C at midday. However, it is not uncommon for temperatures to exceed 40 °C for several days. This synoptic situation strongly influences surface winds. Some shallow cumulus formation is possible, but moist convection, when present, is generally confined to the surrounding mountain ranges. Due to the proximity of the Mediterranean Sea to the east, the formation of a sea breeze is quite common (Jiminéz Cortéz et al., 2023), but its inland propagation is slowed by the presence of the Catalan pre-coastal and coastal ranges that separate the Ebro basin from the sea (Lunel et al., 2024b). The intensity of the westerlies and the strength of the thermal low also contribute to the propagation and intensity of the sea breeze front, which is locally known as the *Marinada* when it reaches the Ebro basin. In general, the sea breeze front arrived during the field campaign between 16:00 and 19:00 local time over the study area from the east, with the dry-zone locations being affected earlier. The passage of the sea breeze was observed as a low-level wind shift (to easterly winds) over the entire region, while horizontal scanning lidar observations also showed a significant increase in low-level moisture. The arrival of the sea breeze generally coincided with the collapse of the atmospheric boundary layer (ABL) in the late afternoon due to reduced surface heating and turbulence. Days with a predicted early arrival of the sea breeze were not designated as IOPs during the daily briefings (see Section 2.2). An IOP was defined a priori as a relatively clear day characterized by a well-mixed ABL with weak synoptic-scale forcing, such that surface-induced local to regional-scale circulations were most likely to be present and detectable.

2.1.2. Summary of SOP weather conditions

The weather during the SOP was close to the average climatological conditions expected for this time of year, with mostly clear skies and little precipitation. The weather conditions early in the SOP (15–19 July) were characterized by clear skies and westerly low-level flow, with maximum daily highs increasing from around 30 °C at the beginning of the period to 35 °C by the end. This was followed by a relatively hot period (20–23 July), which was characterized by clear skies and the formation of a thermal low. Daily maximum temperatures started around 36 °C and increased to 39 °C by the last two days of the period. Over the next two days (24–25 July), maximum temperatures dropped to the lower 30s°C, associated with some high clouds and westerly near-surface winds ahead of an approaching synoptic-scale trough. A rain event occurred on 26 July, associated with the passage of this trough. Local rainfall totals of about 30 mm were recorded over the irrigated zone; however, the convective cells propagated to the northeast, and the dry zone received relatively little rain, reinforcing the wet-dry zone contrast during the following days of the SOP. Maximum air temperatures remained in the upper 20s°C on this day. The next two days (27–28 July) were marked by synoptic-scale anticyclonic conditions with fairly clear skies and a return to daily maximum temperatures of around 32 °C. A thermal low regime was observed on 29 July, with relatively clear skies and temperatures climbing back into the mid-30s°C.

2.2. Forecast support/decisions

A daily briefing was held each morning (09:00 to 12:00 local time), consisting of a review of the previous day's scientific activities and potential technical issues, a forecast briefing, and a final discussion to propose an IOP day two days in advance, confirm it one day in advance, and possibly cancel it on the morning of the IOP (in case of poorly anticipated deterioration of weather conditions or technical issues). Daily forecast briefings were provided by a team of forecasters from the Meteorological Service of Catalonia (SMC) and three students from the National Meteorological School (ENM) of Météo-France. The forecasts were based on operational model output from a version of the Weather Research and Forecast (WRF) model used operationally by the

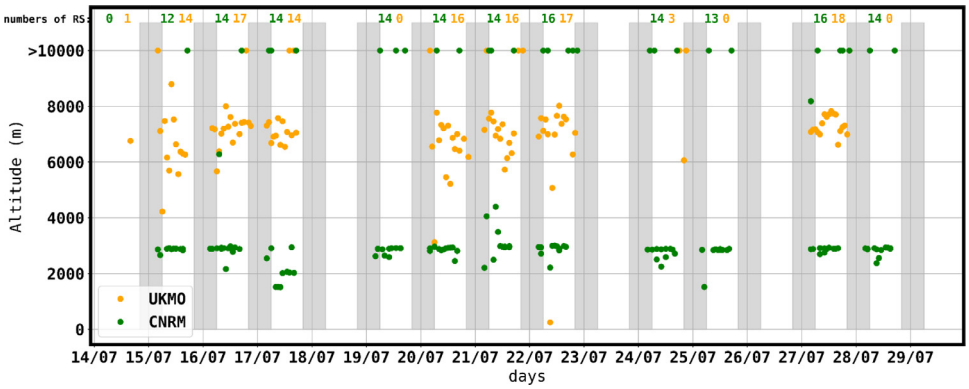

Fig. 2. Time series of available soundings for both the CNRM (green: La Cendrosa) and the UKMO (yellow: Els Plans). The numbers at the top of the plot provide the number of radiosondes per day.

SMC (Mercader et al., 2010), the European Centre for Medium-Range Weather Forecasts (ECMWF), the ARPEGE model (Research Actions from Small to Large Scales: Courtier et al., 1994), and the AROME model (Application of Research at the Operational Mesoscale: Seity et al., 2011), of which the latter two are used and maintained at Météo-France. The operational WRF-ARW (Advanced Research WRF) configuration uses a cascaded grid nesting from 9 to 3 km spatial resolution, but output from a research version running at 1.5 km was also used. AROME (with a domain covering most of Spain) is run operationally at 1.3 km. The other two models are global (with resolutions slightly less than about 10 km over the area). These forecasts were used to coordinate the timing and flight paths of aircraft, various surface-based atmospheric monitoring operations such as tethered balloon operations and radiosonde soundings, and coordination with the teams carrying out surface measurements for the calibration and evaluation of data from airborne sensors.

2.3. Radiosoundings

Radiosondes are essential for sampling the atmospheric state in the vertical. During the SOP, 11 days of favorable conditions with dry convection were documented. Hourly radiosonde releases were done at the two main sites: La Cendrosa (irrigated) and Els Plans (rainfed and dry, see Fig. 1 and Section 2.7). Radiosoundings using Vaisala RS92-SGP receivers were conducted at the Els Plans site. On four evenings, the soundings were extended until 23:00 local time to capture the ABL evening transition. Radiosondes reached a maximum height of 8 km. At La Cendrosa, both Vaisala RS41-SGP (for the first and last releases at 0700 and 1700 UTC) and RS92-SGP (for all other releases) receivers were used. A total of 269 radiosondes were launched, with 11 IOPs (154 radiosondes) at the irrigated site and 7 IOPs (115 radiosondes) at the rainfed site. Reusable radiosondes, developed by the CNRM (Legain et al., 2013), were also used during this campaign at the irrigated site. The reusable radiosonde consists of a conventional version under a set of two balloons inflated differently: one for ascent and one for descent. The carrier balloon is released by a cutting system that triggers at a chosen pressure level, and the radiosonde then falls at a descent rate controlled by the remaining (slowing) balloon. During the LIAISE IOP days, only 35 radiosondes were used (the maximum reuse of one radiosonde was 15 times). A summary of the releases and the maximum radiosonde heights is shown graphically in Fig. 2. These soundings provided a detailed description of the vertical structure of the lower troposphere above each surface. See Brooke et al. (2023) for more details on the radiosounding protocols and analysis.

2.4. Measurements of the properties of the lower atmosphere

Multiple instruments were combined to create a strategy for measuring high vertical resolution profiles of atmospheric properties and turbulence from the surface layer through the lowest few kilometers of the atmosphere at several sites. These measurements are valuable for studying how surface fluxes of heat, mass (water), and momentum interact with the lower atmosphere and influence ABL development.

The properties of the lowest several hundred meters of the atmosphere were measured at La Cendrosa using tethered balloon flights (at heights of 50 to 600 m), which were conducted on IOP days from approximately sunrise to early evening. A vertical profiling Leosphere WindcubeV2 lidar (40 to 250 m) was in operation throughout the SOP. During the SOP at Els Plans, the evening transition soundings were extended into the stable boundary layer by the deployment of a tethered balloon, which provided a total of 67 profiles up to 300–400 m above the surface during nine nights. A 1.5 μm Halo Photonics Streamline lidar was installed to measure radial backscatter and Doppler velocity from the aerosols. The Halo operated in zenith view, so the vertical velocity and the vertical component of turbulence were continuously monitored. A second lidar setup was installed near this site, facing north, with a swath across the transition zone between the irrigated and rainfed zones, providing measurements of state variables and turbulent fluxes. Finally, the lower atmosphere was monitored at Mollerussa using a Radio Acoustic Sounding System (RASS) sodar to provide vertical profiles of wind and virtual temperature between 40 and 300 m a.s.l.

Two ultra-high-frequency (UHF) wind profiler radars were deployed during the summer at La Cendrosa and Els Plans. Both were 1.274 GHz Doppler radars, with five beams (one vertical and four oblique beams, 15° from zenith), which enabled the retrieval of the mean wind profile from 200 m a.g.l. to about 3000 or 4000 m a.g.l., as well as the ABL depth. These radars allowed continuous description of lower tropospheric dynamics and revealed evidence of the entrance of the Marinada, vertical shear, decreases in wind speed within the convective atmospheric boundary layer (CBL) due to dry convection, and free tropospheric flow. Doppler spectra provided access to profiles of the turbulent kinetic energy (TKE) dissipation rates (Jacoby-Koaly et al., 2002) and vertical velocity variance. Recently, Philibert et al. (2024) developed a new algorithm to retrieve the complex structure of the low troposphere based on UHF radar reflectivity and Doppler spectral width, which are related to inversions and dry convection, respectively. This algorithm was used in LIAISE to describe the CBL depth and to detect internal boundary layers, residual layers, or advected boundary layers. Results showed that the CBL is often deeper over Els Plans, consistent with the drier surface and larger sensible heat flux, though not always. The UHF wind profiles were complementary to the corresponding RS measurements for the lower troposphere (albeit with greater vertical resolution).

Precipitation characteristics and related microphysical processes were also studied during the LIAISE field campaign. Previous studies have reported that sharp vegetation contrasts may influence not only

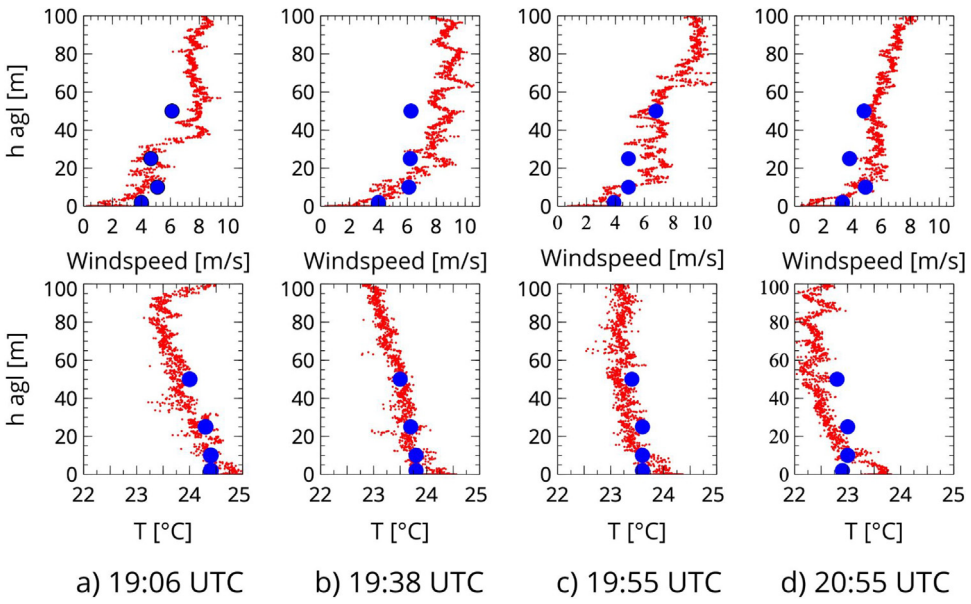

Fig. 3. Tower data (blue circles) and Q17 drone data (red dots) for flights on July 28 2021 in Els Plans with the times indicated in UTC at the base of each panel. The Q17 drone operated by the Ostwestfalen-Lippe University of Applied Sciences and Arts used a Anemoment Trisonica for the measurements.

Table 1
A summary of the atmospheric profile measurements from in-situ (balloon-based or UAVs) or remote sensing. Note that TOA (top of the atmosphere) represents soundings reaching the upper part of the troposphere (>= 10 km altitude) which were released less frequently than the other radiosondes (RS) (see Fig. 2). Further details on the instruments are given in the text.

Surface up to ~100 m	Surface layer up to several 100 m	Surface layer up to the height shown	Surface up to the height shown	200 m to 3–4 km	Location
–	lidar	tethered balloon (600 m)	RS (~3 km) & TOA	UHF	La Cendrosa
UAV	RASS	–	–	–	Mollerussa
UAV	lidar	tethered balloon (400 m)	RS (~8 km) & TOA	UHF	Els Plans

boundary layer characteristics and mesoscale circulations but also convective initiation (Pielke, Sr., 2001; Wang et al., 2011; Huang et al., 2019), which may lead to subsequent heterogeneities in the precipitation field. To assess the possible effects of surface characteristics on precipitation processes, additional instrumentation complementing the operational rain gauge observations and C-band weather radar products covering the area was deployed. In particular, through the cooperation of Météo-France, Université Grenoble-Alpes, and the University of Barcelona, three sites (La Cendrosa, Mollerussa, and Tàrrega SMC) covering both the irrigated and rainfed LIAISE domains were equipped with co-located Micro Rain Radars and PARSIVEL laser disdrometers to observe precipitation particle size and fall speed spectra at ground level and over a 3-km height column with 1-minute resolution. A fourth site (Tordera-AEMET) was also equipped with a laser disdrometer. These data sets allow for an analysis of the microphysical characteristics of precipitation events during LIAISE. Preliminary results indicate similar characteristics of precipitation in both irrigated and rainfed areas, as well as the importance of sub-cloud rainfall evaporation in both (Bech et al., 2024; Polls et al., 2024).

2.5. Unmanned aerial vehicle (UAV) flights

Drone flights were conducted by several institutes during the LIAISE field campaign. The drone activities in July 2021 had four main priorities: (a) analysis of vegetation activity through solar-induced fluorescence (SIF) imaging (6 flights), (b) identification of vegetation stress situations using multispectral and thermal imaging (26 flights), (c) meteorological vertical profiling of wind, temperature, and humidity (36 flights), and (d) support flights to provide high-precision maps and digital elevation models (5 flights). Some of the flights, such as the SIF flights, were closely coordinated with manned flights. The significance of SIF is that it can serve as a proxy for photosynthesis and transpiration. The drones proved to be valuable and complementary tools alongside ground-based and other airborne systems (e.g., balloons, manned aircraft). Fig. 3 shows data from the tower at Els Plans (blue circles) and data acquired by the Q17 drone on July 28, 2021, at Els Plans. For information on the Q17 and its instrumentation, see Wrenger and Cuxart (2024). The flights shown in Fig. 3 were performed as part of an inter-method comparison using the tower operated by the UKMO as the reference and thereby ensure the data quality of the UAV flights. The choice of this day was mainly for two reasons. First, from a pragmatic standpoint, the 28th was near the end of the SOP and most of the measurement objectives had been attained thus there was additional time to make these flights. Second, the goal of the flights were to capture the evening transition (in terms of going from unstable to stable near surface conditions) and the anticipated weather conditions were relatively calm and anticyclonic and thus favorable (see Section 2.1.2). Finally, a UAV was used at Mollerussa to obtain profiles of the lower atmosphere. Several UAV flights equipped with multispectral and thermal imaging cameras were also conducted to evaluate the performance of the thermally based two-source energy balance (TSEB) model for estimating diurnal ET and its partitioning components. A list of the sites that had UAV flights for measuring the properties of the lower atmosphere, along with other measurements of the lower atmosphere, is summarized in Table 1.

2.6. Aircraft based measurements

Three manned aircraft were flown over the LIAISE study zone during the SOP period (15–29 July, 2021). They included instrumentation

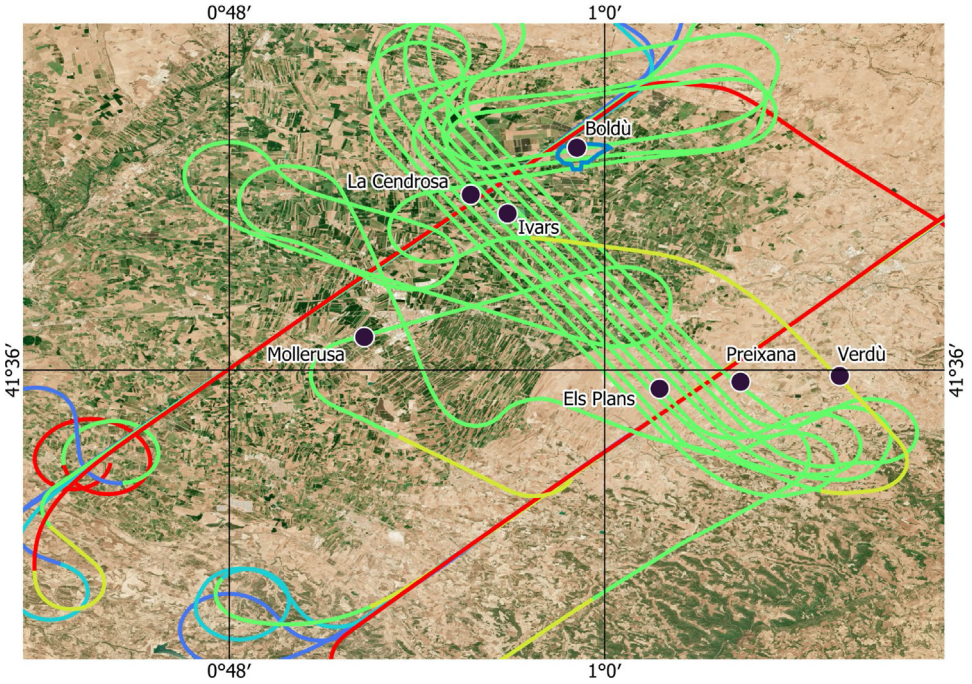

Fig. 4. Flight paths for the ATR42. The red flight lines running from the southwest to the northeast correspond to the (first) turbulence leg of the flight (at 5 stacked vertical levels) over the irrigated and rainfed zones. The 9 transverse parallel (green) flight lines running from northwest to southeast correspond to the (second) constant altitude surface (GLORI and HyPlant) scanning leg. A summary of the flights is given in Table 2. The GLORI soil moisture product was evaluated using data from a soil moisture monitoring network containing the Boldú site (blue outlined region).

to characterize the atmospheric state, to make turbulence measurements and to estimate various surface properties. The objectives and complementarity of these flights are described in this section.

2.6.1. Atmospheric state and turbulence

The French Office of Aircraft Instrumented for Environmental Research (SAFIRE) ATR-42 (*Avions de Transport Régional*: Regional Transport Aircraft) aircraft flew intensively in the LIAISE field campaign region, equipped with instruments capable of measuring high-frequency wind, temperature, and humidity data to document the characteristics of the ABL above the LIAISE study area. Details about the instrumentation and processing are provided in Saïd et al. (2010), Brilouet et al. (2021), and Bony et al. (2022). The aircraft explored the atmosphere above two areas: irrigated (wet) and rainfed (dry). The flight paths over the LIAISE study area are shown in Fig. 4. Atmospheric state and turbulence legs, each 35 km long, were first flown around midday at five stacked vertical levels ranging from 300 m to several kilometers in height, within and above the ABL (indicated by the red lines running southwest to northeast). Next, the ATR-42 made 9 transverse, nearly constant-altitude flights (at a height of approximately 1150 m) that crossed the interface between the wet and dry areas, as indicated by the parallel green lines. These are referred to as the GLORI-HyPlant scanning legs. The Global Navigation Satellite System Reflectometry Instrument (GLORI), developed and maintained by CESBIO, was installed on the SAFIRE aircraft. It was used to generate a complete set of Global Navigation Satellite System Reflectometry (GNSS-R) airborne data, which provided an estimate of surface soil moisture (SSM) at a 100 m resolution. The HyPlant sensor, a high-performance airborne imaging spectrometer operated by Forschungszentrum Jülich, was used to retrieve the SIF from the high-resolution HyPlant radiance data. See Section 2.6.2 for further details on the GLORI and HyPlant instruments. The focus of these legs was on scanning the surface properties, although atmospheric measurements were also taken. See Table 2 for a summary.

A 5 km high-pass filter was applied to the 25 Hz time series to remove mesoscale variability. The fluctuations in vertical wind, potential temperature, and water vapor mixing ratio are denoted as w', t', and q', respectively, along the stacked legs. The turbulent moments associated with these fluctuations were calculated for each leg. The kinematic sensible and latent heat flux profiles, denoted by $\langle w't' \rangle$ and $\langle w'q' \rangle$, respectively, are shown in Fig. 5. These profiles were estimated within and above the ABL by the ATR-42 research aircraft on July 15, 2021. The profiles are supplemented near the surface by estimates from a 50 m instrumented mast and a tethered balloon-borne turbulence probe. In this example, the highest thermal production is identified in the dry region, with the kinematic sensible heat flux, $\langle w't' \rangle$, being twice as large compared to the moist region. The moisture flux, $\langle w'q' \rangle$, is approximately zero in the dry zone and positive in the wet zone, reflecting the strong contrast in water content between the two areas. This example also shows the complexity of the exchange between the two areas, with a positive moisture flux observed over the top of the ABL. Additional legs were flown by the ATR-42 at a constant altitude (1150 m a.g.l.), crossing the two areas (irrigated and rainfed). These transverse legs can also be used to estimate turbulent moments and should be useful in understanding the horizontal transport of heat and moisture between the wet and dry zones.

Note that at the beginning of the SOP, there was no marked difference between the two areas in terms of near-surface turbulence (and thus the ABL depth, as seen in Fig. 5). However, complementary analyses (not shown) revealed a complex lower troposphere over the wet area on several other SOP days, with fairly strong turbulence detected above the surface-coupled mixed boundary layer (the top of the ABL was determined through a synergy of several remote sensing and radiosonde methods). This mixed layer was shallower, cooler and less turbulent over the irrigated area than in the dry zone, while also being overlaid by another turbulent layer. This may be interpreted as either an internal boundary layer and/or as the advection of the neighboring, drier, and deeper boundary layer above this wetter mixed layer.

Table 2
List of the 8 ATR-42 flight dates, number of legs done above the arid area/above the humid area from one side to the other, median time over the considered duration of the flight, and estimates of mean ABL depth (*Zi*) from UHF wind profilers using the CALOTRITON algorithm (Philibert et al., 2024) or radiosoundings.

Date (year-month-day)	Numbers of legs arid/humid/GLORI	Mean flight time (UTC)	Average *Zi* arid/humid zone (m)
2021–07–15	5/5/9	12:30	700/750
2021–07–16	5/5/9	12:00	700/600
2021–07–17	5/5/9	14:00	650/450
2021–07–20	5/5/9	12:00	1350/1750
2021–07–21	5/5/9	12:00	400/300
2021–07–22	5/5/9	14:00	1750/1700
2021–07–27	5/5/9	13:30	1200/1250
2021–07–28	5/5/9	13:30	1500/600

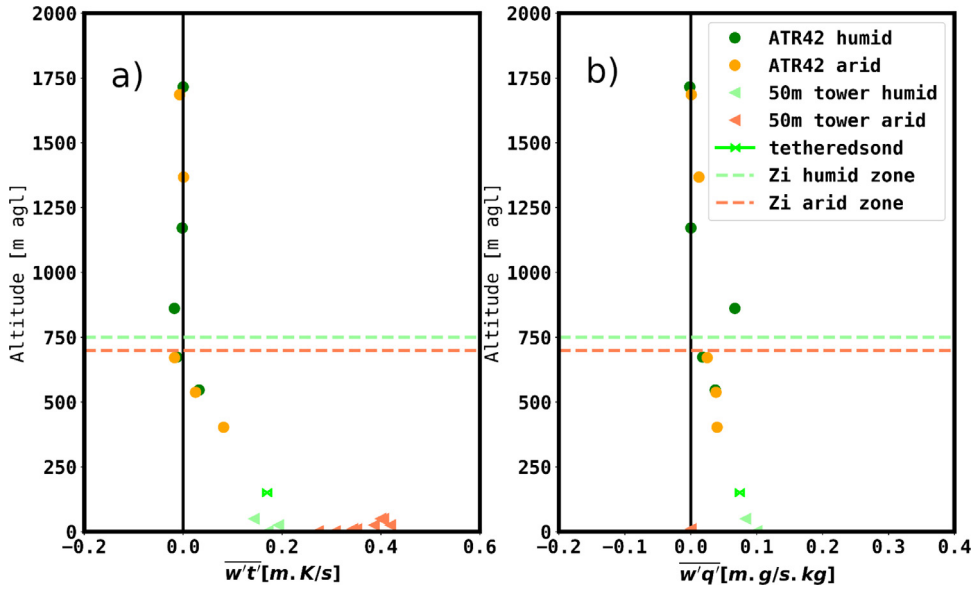

Fig. 5. Vertical profile of kinematic (a) heat flux and (b) moisture flux observed on July 15 2021. Orange and green symbols denote the two different explored areas, arid (rainfed) and humid (irrigated), respectively. Dashed lines represent the ABL top (*Zi*).

2.6.2. *Aircraft-based remote sensing of surface properties*

SSM has been identified by the Global Climate Observing System (GCOS) as an essential climate variable, crucial for characterizing the Earth's climate. Recently, numerous SSM products and approaches have been developed, based on the use of passive radiometers (e.g., SMOS, SMAP, or AMSR-E) or active synthetic aperture radars (SARs) and scatterometers (e.g., ERS, ASCAT, Sentinel-1, Radarsat, TerraSAR, ALOS/PALSAR, or SAOCOM). SSM maps obtained from the airborne GLORI GNSS-R on board the ATR42 were developed during the SOP phase of the field campaign. The SSM mapping is based on the ΓRL map at 100 m resolution (Zribi et al., 2022). The inversion model was applied to each grid, incorporating both Γ_{RL} (reflectivity) information and NDVI calculated from Sentinel-2 data. Maps of volumetric water content (m^3 m^{-3}) were generated for flights on July 22, 2021, and July 27, 2021 (after a precipitation event), as shown in Fig. 6. In both cases, a clear contrast between irrigated and rainfed areas was observed, with higher moisture levels in the irrigated areas. Reflectance and ground truth measurements are available in the LIAISE database, as described in Dassas et al. (2024). While coarse spatial resolution SSM products have been evaluated over a wide range of ecosystems, there is a lack of comparative studies for the very high spatial resolution (a few meters) products that have become available in recent years. LIAISE provided a unique opportunity to evaluate the accuracy of these high-resolution SSM products (Ouaadi et al., 2024). The evaluation showed that products derived from active microwave data (radar) generally outperformed products based on the disaggregation of coarse-scale SSM products. Interestingly, some areas that were drip-irrigated by the Segarra-Garrigues Canal outside the main irrigation zone (in areas enclosed by black rectangles in Fig. 6) had relatively high SSM values in the GLORI product, which were not seen in the disaggregated product presented in Ouaadi et al. (2024), probably due to the fact that the vegetation was poorly developed. Finally, Ouaadi et al. (2024) highlighted the limitations of SSM products over tree crops and the open perspectives for the improvement of irrigation scheduling—determining when and how much water to apply to a field—using the high spatial resolution LIAISE data.

An additional instrument was installed on the ATR42 to estimate another surface property: fluorescence, or the re-emission of light by plants, which can serve as a proxy for photosynthesis and transpiration. The great potential of this technique is that it can be remotely sensed from space. Seven airborne image data sets of the LIAISE study region (~77 km^2) were acquired with HyPlant in July 2021 (July 15–17, 20–22, and 27). The data sets were acquired between 13:00 and 17:00 local time (CEST) at an altitude of 1150 m, with a spatial resolution of 1.7 m. The HyPlant sensor is a high-performance airborne imaging spectrometer consisting of two sensor modules. The DUAL module comprises two imaging line scanners that provide spectral information from 380 nm to 2500 nm, while the FLUO (fluorescence) module has much finer spectral resolution (0.25 nm: Rascher et al., 2015). Within the processing chain (described by Siegmann et al., 2019), the SIF is retrieved from the high-resolution HyPlant FLUO radiance data using a dedicated spectral fitting approach (Cogliati et al., 2019). As final products, top-of-canopy reflectance and vegetation index maps were derived from HyPlant DUAL data, while red (687 nm) and far-red (760 nm) SIF maps were derived from HyPlant FLUO data. Fig. 7 shows an example of a recorded image mosaic consisting of nine flight lines

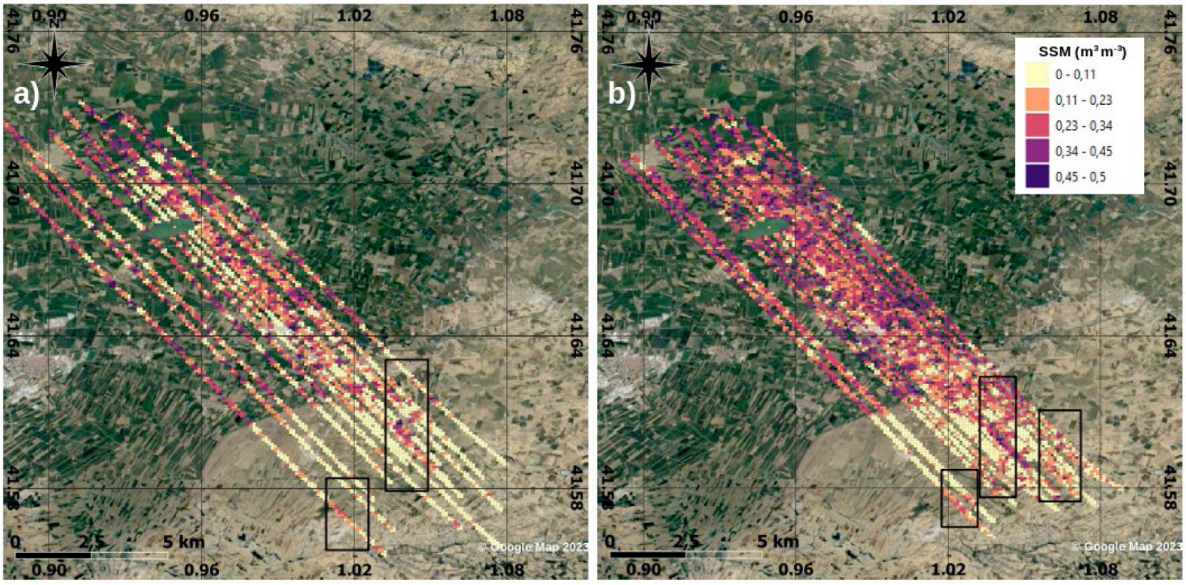

Fig. 6. SSM maps (100 m spatial resolution) retrieved from the Γ_{RL}(reflectivity) inversion: (a) Flight 45 on 22 July 2021 during dry conditions, (b) Flight 46 on 27 July 2021 which was relatively wetter after a precipitation event. The boxes indicate zones containing fields with drip irrigation (pixels with relatively larger SSM) which were not seen by disaggregated SSM products. The background map is from Google Map (last accessed in 2023).

recorded on July 17, 2021. Fig. 7a shows an NDVI map derived from HyPlant DUAL top-of-canopy reflectance data, and Fig. 7b shows a far-red SIF map derived from HyPlant FLUO data at 760 nm. While the NDVI map serves as a proxy for the amount of available green biomass, the SIF map provides information about the plant's photosynthetic performance at the time of data recording.

A second aircraft, a B200 King Air, was flown by NASA with the Scanning L-band Active Passive (SLAP) sensor on board to provide soil moisture (SSM) estimates over both irrigated and rainfed areas. Most flights were conducted at low altitude (300 m), providing a unique opportunity to obtain small 100 × 200 m footprints. Two flights were conducted at medium altitude (approximately 800 m) to provide a broader context. The data products include passive brightness temperature, active backscatter coefficient, and soil moisture (from the passive measurements). See Kim et al. (2023) for a detailed description of the methodology and available data products over the LIAISE study area.

A third aircraft, the Flying Laboratory of Imaging Systems (FLIS), an airborne infrastructure operated by Czechglobe, performed five successful flights. Visible, near-infrared, and thermal infrared hyperspectral imaging sensors were used to acquire data of target areas under different viewing angles. The study primarily focused on investigating the Bidirectional Reflectance Distribution Function (BRDF) effect.

2.7. Ground based flux sites and supersites

Seven observation sites were equipped with ten SEB stations (one site, Mollerussa, included SEB stations over three different vegetation types, and another, La Cendrosa, had two SEB stations over the same land cover). All SEB stations used eddy covariance to compute turbulent fluxes in addition to the main components of the surface radiation budget. The corresponding instruments are listed in Table 3, along with information on soil temperature and moisture measurements. The location of the study area allowed the project to benefit from dense local meteorological station data and radar data from SMC, as well as an existing extensive observation site operated by the Institute of Agrifood Research and Technology (IRTA) and SMC in Mollerussa. Three of the sites were located above cultivars in the wet (irrigated) zone, three were in the dry zone (one of which was drip-irrigated), and the final site was a lake in the wet (irrigated) zone. Leaf and canopy-level ecophysiological data were collected for five vegetated SEB sites. Additionally, two thermo-hygrometers were installed within aspirated radiation shields at two levels close to the surface to assess the flux-gradient approach (Martí et al., 2022) in estimating surface turbulent fluxes over six different surfaces using the Businger-Dyer functions (Dyer and Hicks, 1970). The first site analyzed was Els Plans, where the estimation of latent heat flux required newly adjusted functions when the sensible heat flux was dominant due to the relatively dry soil. Field-scale turbulent flux estimates from scintillometers were made at three of the sites (Mollerussa, Ivars Lake, and La Cendrosa; see Section 2.8). Finally, two sites (La Cendrosa and Els Plans) were complemented by extensive measurements of the lower atmosphere using captive balloons, frequent radiosoundings, UHF wind profilers, lidars (see Section 2.4), and nearly identical 50 m towers (Fig. 8). Micro-lysimeters were used to determine the daily patterns of soil evaporation and their spatial variability at four sites (Mollerussa, La Cendrosa, Preixana, and Verdú) on specific days of the SOP. Ecophysiological measurements at both the leaf and canopy levels were performed at all field sites within the LIAISE domain with the aim of providing vegetation-specific parameters for LSMs, estimating leaf and canopy traits as ground truth for remote sensing and eddy covariance measurements, quantifying diurnal patterns of leaf transpiration in response to drought stress, and quantifying the partitioning of ET between plant transpiration and soil evaporation, as well as the net carbon fluxes between plant photosynthesis, plant respiration, and soil respiration. A summary of the irrigation method, cover type, and height is provided in Table 3.

A unified flux dataset for the SOP was produced using a standard approach, which involved using the flux software package EddyPro version 7 (Fratini and Mauder, 2014) from LI-COR Biosciences Inc. (Lincoln, Nebraska, USA) to calculate the turbulent fluxes with both 10- and 30-minute averaging times. The missing data threshold was set at 10% per period. All standard data treatment and flux correction procedures were applied, including axis rotation using the planar-fit procedure (Wilczak et al., 2001), raw data screening with spike removal (Vickers and Mahrt, 1997), interval linear detrending, and low-pass filtering correction (Massman, 2000), as well as time lag correction with covariance maximization and WPL density correction (Webb et al., 1980). In addition, quality flags were determined based on Mauder and Foken (2004). No gap filling was applied. In addition, the processing of the individual datasets (sometimes covering a longer time period) was similar, but there are some differences in the details which can be

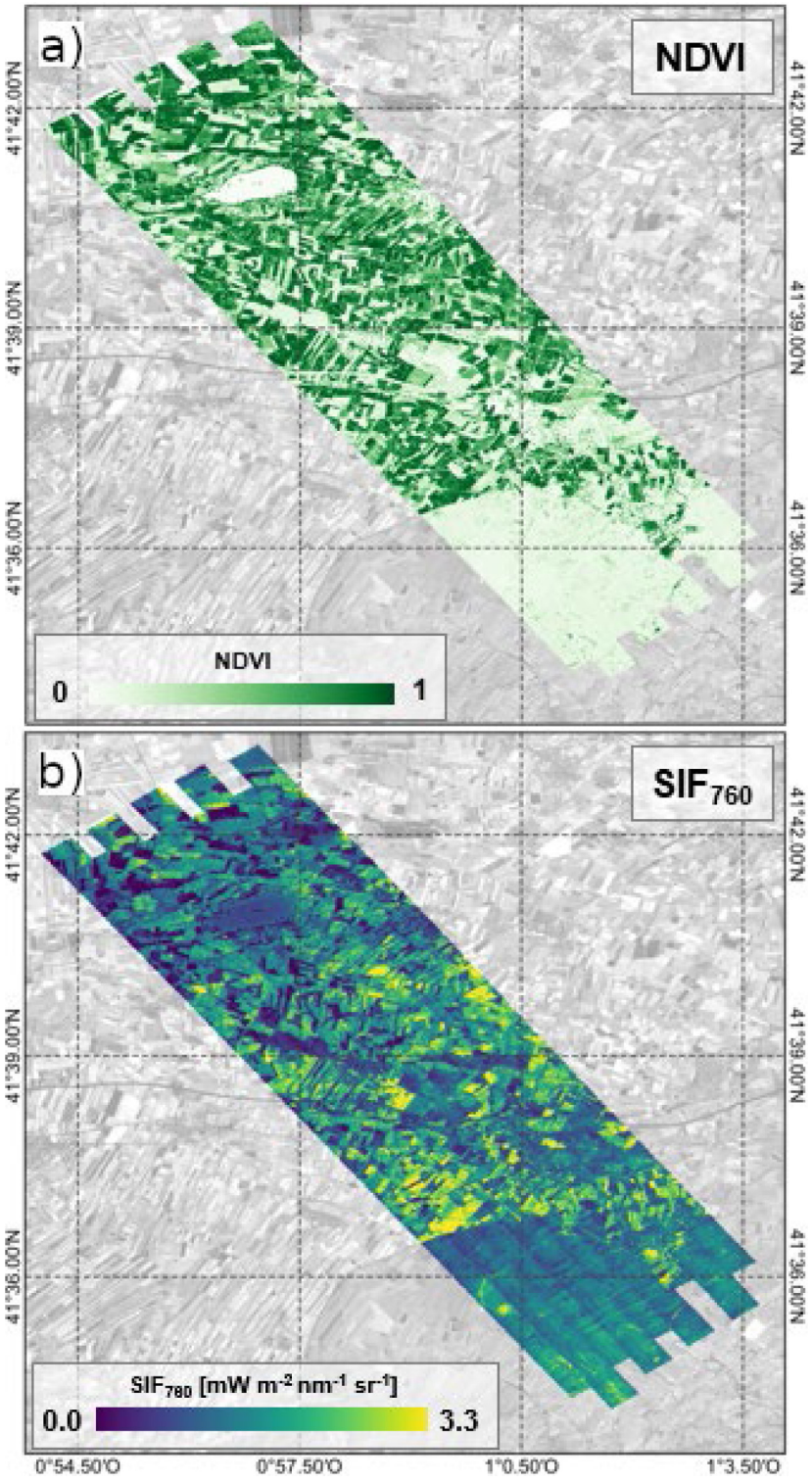

Fig. 7. Mosaic of nine HyPlant flight lines recorded on 17 July 2021. (a) HyPlant NDVI map and (b) far-red solar-induced fluorescence (SIF_{760}: mW m^{-2} nm^{-1} sr^{-1}) map.

found in the meta-data description of the data which is available on the LIAISE database site (https://liaise.aeris-data.fr/).

2.7.1. La Cendrosa: Irrigated alfalfa (Wet Area)

The La Cendrosa supersite was irrigated just before and once during the SOP using the flood/gravity method. The crop was mown just before the SOP began, leaving the stubble height (a few cm) sparse so that a significant bare soil fraction was visible. However, after an irrigation event, the alfalfa grew at a rate of nearly 0.04 m day^{-1}, and it was ready for mowing just before the end of the SOP, reaching a height of about 0.7 m. A 50 m mast was installed with air temperature and relative humidity measurements made using Thermoest PT100 and Vaisala HMP110 sensors, located at 0.2, 2, 10, 25, and 45 m. Four-component radiation measurements at 1 m were obtained with a Kipp and Zonen CNR4 net radiometer. Precipitation was measured with a Précis Mécanique 3039. A SEB station was installed to measure meteorological variables at three levels and allow turbulent flux calculations

Table 3
Instruments at the selected SEB stations with cover type and irrigation method (N.A. represents non-applicable or not measured). CSAT3, EC150 and Krypton are Campbell Scientific (CS) Instruments; LI stands for LI-COR, RM for Young, HS-50 and R3-50 are Gill models, CNR1, CNR4, CRg4 and CM21 are Kipp & Zonen devices, NR01 and flux plates are made by Hukseflux, SN500-SS by Apogee. There were two SEB stations over the same land cover at La Cendrosa, and there were three SEB stations for different land cover types at Mollerussa. The instrumentation used for both soil temperature and moisture along with the soil depths are shown for corn at Mollerussa. At Boldú, SEB measurements were lifted once as the corn grew (reset to 2 m above the canopy). "Irrig-Meth" represents the irrigation method, and "spkle" refers to the use of a sprinkler system for irrigation.

Site	Land Cover	Irrig-Meth	Sonic and gas analyzer & height (m)	Net radiation & height (m)	Flux plate depth (cm)	Canopy height (m)	Soil temperature, depths (cm): soil moisture, depths (cm)
La Cendrosa	alfalfa	flood	Gill R3-50, LI7550, 3.0	CNR4, 1.0	3	0.1–0.8	Generic Pt100, 5, 10, 30: Delta T Thetaprobe ML3, 5, 10, 30
La Cendrosa	alfalfa	flood	IRGASON& LiCor7500, 1.0	CM11 & CG2	5	0.1–0.8	Generic Pt100, 2, 10: N.A.
Verdú	vinyard	drip	IRGASON, 4.0	Apogee SN500-2SS, 3.5	3	1.5	T107, 5: DeltaT ML2x, 5, 20, 40
Mollerussa	corn	flood	CSAT3, EC150, 3.3	NR01, 2.9	8	2.7	CS-SoilVUE10, 0, 5, 15, 25, 35, 45
Mollerussa	apples	drip	RM81000, Krypton, 5.1	NR01, 4.4	8	3.0	Thermistors 107/ CS650, 1.5, 3.5, 5, 17, 23: Campbell CS650/5, 8, 22
Mollerussa	cut grass	spkle	CSAT3, LI7500, 2.0	CNR1, 1.0	8	0.1	Campbell TCAV, 2, 8: Campbell CS616, 2.5
Preixana	almond	none	HS-50, LI7550, 7.3	CNR4, 1.0	3	4.0	Euro Pt1000, 5, 10, 30: Delta T Thetaprobe ML2x, 5, 10, 30
Els Plans	natural grass	none	HS-50, Krypton, 2.0	CRg4/ CM21, 1.0	2	0.3	Delta T ST2 0.5 m, 1, 4, 10, 17, 35: Delta T ML3, 10, 20, 30, 40
Lake Ivars	water	N.A.	HS-50, LI7500, 3.0	CNR4, 1.0	N.A.	N.A.	N.A. : N.A.
Boldú	corn	flood	CSAT1/ LI7500, 2.0–4.0	NR1, 2.0–4.0	8	0.3–2.4	CS107, 5 10, 20, 40: CS616 reflectometer, 20, 40

at two heights from April to October. Sonic and gas analyzers are listed in Table 3.

Before applying the eddy covariance method, several checks were performed to eliminate isolated peaks and highly anomalous values using simple statistical checks. The eddy covariance method was then used to calculate the turbulent fluxes, following these steps: (i) despiking using a variance threshold for each parameter, (ii) a 2-D rotation that first aligns the coordinate system with the mean wind and, in a second step, accounts for the inclination of streamlines to yield a zero mean vertical wind speed, (iii) detrending, and to eliminate the signal from movements slower than turbulence, a low-pass filter was applied, (iv) maximum covariance was used to reduce errors caused by the distance difference between the sensors, and (v) a spectral correction for high-pass filtering effects (Moncrieff et al., 2004) was applied. This CNRM-based algorithm was evaluated daily at another station, compared with fluxes computed using the open-source software LI-COR EddyPro (https://www.licor.com/env/support/EddyPro/software.html), and a correlation of 0.99 between the two methods was obtained.

A second eddy covariance system (listed in Table 3), consisting of a CSAT3 sonic anemometer with an integrated open-path infrared gas analyzer, was deployed to the east of the 50 m tower within the alfalfa field. A laser scintillometer was installed for parcel-scale sensible heat flux estimation (see Section 2.8 for details). A four-component radiation sensor was also installed and is listed in Table 3. Diffuse shortwave radiation was measured using the CM11 with a shadow ring. Three micro-lysimeters were used over a 24-hour period to determine diurnal patterns of soil evaporation, nocturnal dew formation, and to separate the ET measurements made by the eddy covariance towers into evaporation and transpiration (Quade et al., 2019). A variety of ecophysiological measurements were made at the plant and leaf level, including in situ measurements of vegetation fluorescence (both passive and active fluorescence and gas exchange), CO_2 assimilation of photosynthetically active radiation (A-PAR), stomatal conductance, photochemical yield, fluorescence (fraction of absorbed photosynthetically active radiation or F-PAR), chlorophyll content, vegetation height, leaf reflectance, leaf area index, and water and carbon isotopes. Canopy profile measurements were also taken, consisting of a network of PAR canopy profiles (18 sensors), four ATMOS 2D sonic sensors (at 29, 58, 100, and 162 cm), and five Deacgon temperature-humidity probes (at heights of 10.5, 24, 61, 99, and 149 cm). A distributed temperature sensing (DTS) Raman scattering optical cable (SiliXa Ultima M) was also installed along the central 50 m mast and across the field. The DTS technique is based on the temperature dependence of Raman backscattering in a fiber optic cable, providing spatially distributed temperature data over time. Four DTS setups were deployed at La Cendrosa during the SOP. The first three setups were part of a 600 m long, 1.6 mm thin, Kevlar-reinforced fiber that measured temperature at 5 s and 25.4 cm resolutions to obtain: (1) a surface layer profile between 1.6–40 m with a 25.4 cm vertical resolution, (2) a canopy profile averaged horizontally over 2.5 m with cables at 8 vertical levels between 0–1 m height inside the rapidly growing alfalfa, and (3) a soil profile between −0.48 - 0 m with a vertical resolution of 1.25 cm; the enhanced spatial resolution was achieved by winding the cable into a coil installed in the soil. The fourth setup was a so-called "turbulence harp", which used a thinner, faster optical cable (0.5 mm) over a horizontal distance of 70 m, measuring at four heights between 0.40 m and 2.05 m. Measurements were made at 1 Hz (effective response time of 0.15 Hz) with a 12.7 cm resolution, allowing the spatial structure of turbulence to be studied in terms of spectral analysis and the spatial turbulence statistic, CT^2, which represents the temperature structure parameter.

SIF was observed remotely from UAVs using red, green, and blue (RGB) and multispectral instruments (see Section 2.5), in part to verify airborne SIF measurements from the ATR42 aircraft. Passive SIF and active measurements (Lidar Induced Fluorescence) were performed on site at the La Cendrosa site from July 9 to 29. The objective was to compare the results with the airborne fluorescence measurements made

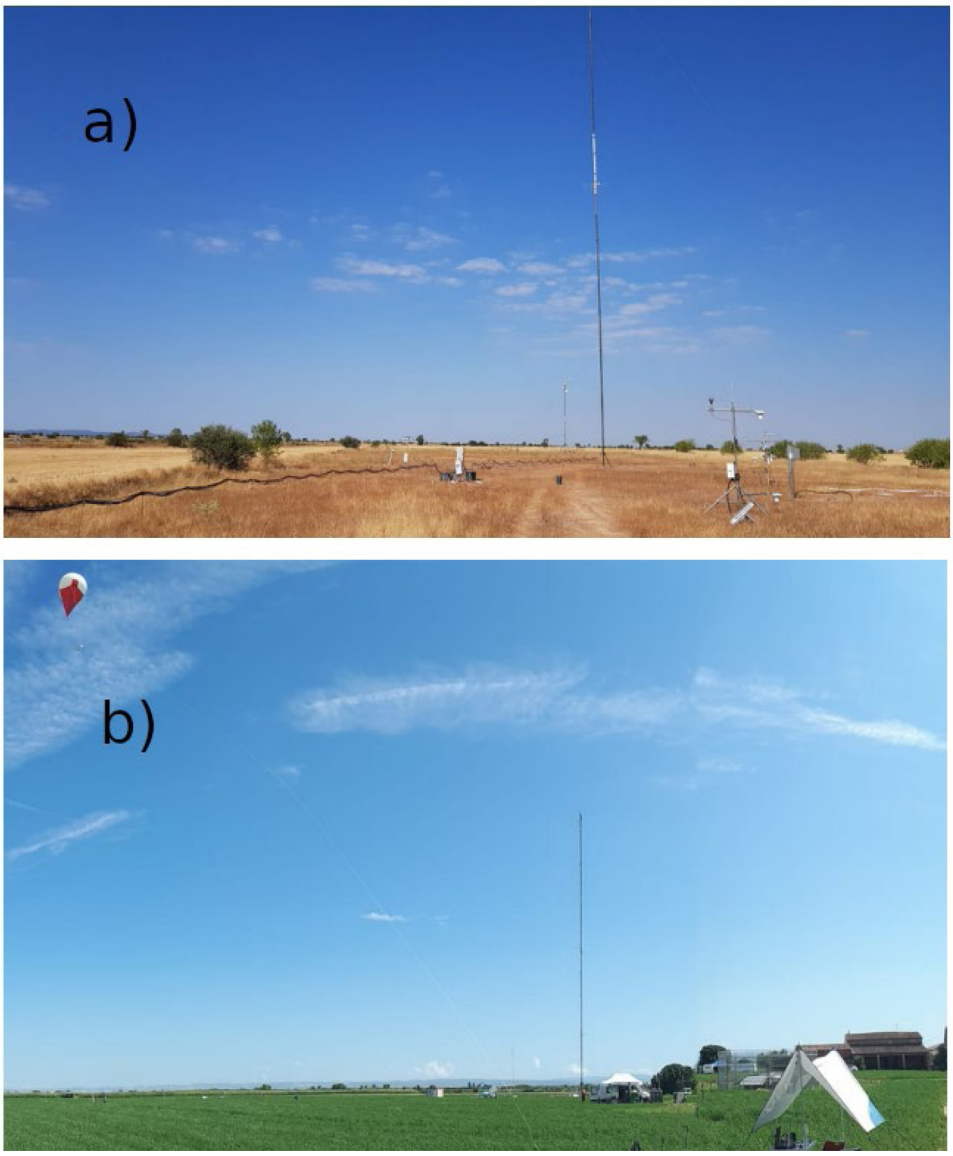

Fig. 8. An example of the surface contrast during the SOP (July, 2021) between the dry area in panel (a) corresponding to the rainfed site at Els Plans, and the wet area in panel (b) corresponding to irrigated alfalfa at La Cendrosa (note that the right hand side of this image has been modified to include the UHF and the tethered balloon operations tent). Each site included measurements along a 50 m tower (shown) along with other instruments described in Section 2.7.

with the HyPlant airborne instrument and to better understand the factors influencing the fluorescence signal under natural conditions. This alfalfa field was mowed at the beginning of the campaign and irrigated once during the campaign, providing good conditions for studying the effects of growth and irrigation on fluorescence. The "low-cost" instruments (SIF and micro-lidar) were installed to point at the same target to allow for a better interpretation of the effect of fluorescence yield on the SIF signal. Measurements at the canopy level were complemented by fluorescence and gas exchange measurements at the leaf level: (i) continuous measurements of fluorescence, fluorescence quenching parameters, photosystem II photochemical yield, and linear electron transfer rate were made at the leaf level using a Monitoring-PAM (Walz, Germany) equipped with two measuring heads and a Fluorpen, (ii) measurements of leaf fluorescence spectra under natural illumination, (iii) joint measurements of fluorescence and gas exchange under controlled illumination with the Licor 6400-XT (light saturation curves of assimilation and fluorescence), (iv) measurements of leaf chlorophyll content (SPAD, Minolta). In addition, measurements of leaf and canopy spectral properties (ASD FieldPro4) and measurements to describe the 3D structure of the alfalfa canopy were performed to test canopy radiative transfer models and to better understand the effect of canopy structure on the fluorescence signal at the canopy (and plot) scale.

2.7.2. Mollerussa: Irrigated apple orchard, corn field and short grass (Wet Area)

The Mollerussa site was located at the IRTA experimental facility, southwest of the city, and included three separate SEB stations, each located over contrasting vegetation types. A particular focus was on ET estimates, which directly contributed to the WCRP-supported Global Energy and Water Cycle Experiment (GEWEX) ET initiative (Cuxart et al., 2019).

The first site is located in a drip-irrigated apple orchard, which was irrigated using two different strategies (full and stressed) during the IOP campaign. A SEB station (see Table 3) was installed above the weighing lysimeter in the water-stressed part of the orchard to provide ET estimates using two different approaches. Additional sensors installed at the tower site (compared to those shown in Table 3) included a Gill WindSonic 2D anemometer at a height of 3.65 m above ground level, two thermo-hygrometers (CS HygroVUE5) housed inside

aspirated CSAT3/Licor 7500 radiation shields at heights of 4.9 m and 3.5 m above ground level, one barometer (CS 106), and one Meter leaf wetness sensor within the canopy to monitor dew formation on leaf surfaces. Soil evaporation was measured over a 24-hour period using three micro-lysimeters. Numerous ecophysiological and leaf and canopy spectral property measurements (using an Analytical Spectral Devices ASD FieldPro4) were also carried out, many of which were the same as those in La Cendrosa. However, some specific experiments were designed to contrast certain processes in well-irrigated versus sparsely irrigated plots, such as stomatal conductance in the apple orchard. Two sets of soil sensors were deployed on either side of the irrigation line, each consisting of temperature measurements at multiple levels. Infrared temperature and PAR sensors were also installed above the apple trees to monitor continuous canopy transpiration and below the trees to measure the bare soil. An automated weather station from the SMC network was maintained a few meters north of the apple orchard.

A second SEB station (see Table 3) was installed in the middle of a maize field (250 × 120 m^2) just east of the apple orchard. The mast was placed on an elevated 2-meter-wide strip of land oriented east–west, separating two identical agricultural plots. The station operated continuously for 9 weeks, from June 26 to September 4, with the maize variety irrigated by flooding twice during the SOP, on July 18 and 27. The rapid growth phase of the plant ended around mid-July, leaving a canopy height that remained almost constant at about 2.7 m during the SOP. Wind speed, water content, sonic temperature, and CO_2 concentration were recorded. Net radiation was measured at 20 cm above the canopy, and standard meteorological data, such as temperature and humidity, were collected inside two aspirated radiation shields at canopy height and 28 cm above it. Additionally, a 2D sonic anemometer (Gill WindSonic) was installed 38 cm above the canopy top. A comprehensive set of soil measurements was also taken between the crop rows. This measurement system included a time-domain reflectometry (TDR) soil moisture and temperature profile sensor (CS SoilVUE10) with measurements taken at five levels from the surface to 45 cm deep, along with two heat flux plates (see Table 3).

Finally, for the LIAISE campaign, a third SEB station was installed over a well-irrigated short grass area (with no soil water stress) to monitor the so-called reference evapotranspiration (ET_0). The instrumentation is listed in Table 3. This SEB station has been in operation since the LIAISE field campaign and is maintained by SMC. Additionally, an optical microwave scintillometer was installed to provide field-scale turbulent fluxes (see Section 2.8 for details).

2.7.3. Boldú: Multiple irrigated crops (Wet Area)

This site contained a mosaic of crops during the 2021 growing season. On May 31, 2021, an open-path energy balance station was installed in a large flood-irrigated corn field. The crop was flood-irrigated approximately every two weeks to receive optimal water inputs. Instruments were mounted on a 4 m mast, and the eddy covariance method was used to estimate mean 30-minute surface fluxes (see Table 3). Standard meteorological data were also collected using high-quality CS instruments, including air temperature, humidity, and pressure. At the time of installation, the corn canopy was fully open and approximately 0.3 m high. A suitable site was chosen based on prevailing wind conditions and an ideal upwind footprint to maintain representativeness. A small clearing was made to prevent the tall maize plants from interfering with the station later, but this clearing was kept as minimal as possible. By June 23, the canopy was 95% closed and had reached a height of approximately 1.4 m. The plants reached maturity, with a final height of approximately 2.4 m, by July 18. Due to the pandemic, it was not possible to travel to adjust the height of the sensors to match the rapidly growing canopy: instruments were raised once. As a result, reliable data were only available until early June, though the main growth cycle was captured.

In collaboration with a local irrigation consulting company, SAF-Sampling, a network of soil moisture sensors was installed over different crops in Prat de Boldú. The objectives of this experiment were multiple: (i) to test an innovative low-cost soil moisture monitoring network; (ii) to provide validation data for estimating soil moisture using GLORI and the Sentinel-1 algorithm; and (iii) to improve an irrigation retrieval algorithm based on satellite data. In agreement with the Cooperative of Ivars, a network consisting of two gateways and 14 soil moisture stations was installed. The site was characterized by cereals (barley, wheat, maize), vegetables (peas, broccoli), forage (alfalfa), and apple trees. Irrigation methods included flooding, sprinklers (pivot, ramp, and full cover), and drip irrigation for broccoli.

2.7.4. Ivars Lake: (Wet Area)

A SEB station (see Table 3) was deployed on Ivars Lake in the irrigated area near the La Cendrosa supersite from May to October 2021. The lake had a surface area of about 2 km^2 (approximately 1 × 2 km in dimension) and was 1–2 meters deep during the LOP. The platform was positioned in the middle of the lake and was powered by a combination of a fuel cell and solar panels. It moved along the lake surface over a small area. Lake water temperature measurements were taken at depths of 0.05, 0.10, 0.30, 0.50, 1.00, and 1.50 m, along with periodic measurements of lake turbidity. Low-frequency (every minute) measurements of temperature, humidity, and wind were recorded at several levels in the lake and in the atmosphere to study processes at the lake/atmosphere interface. The sonic anemometer and humidity sensors were coupled with an inertial motion sensor (100 Hz Mti-G from Xsens) to correct the wind for platform motion. Two canopy-level meteorological stations were installed on opposite sides of the lake near a large optical aperture and a microwave scintillometer (installed and maintained by the University of Wageningen and Research (WUR) group during the SOP; see Section 2.8 for details). Turbulent flux measurements were made over the lake and compared with eddy covariance measurements from the floating SEB station. Finally, several UAV flights were conducted to map the surrounding topography for high-resolution modeling studies (see Section 2.5 for more details on UAV flights).

2.7.5. Els plans: Winter crops and seasonal bare soil (Dry Area)

This site is located in a naturally rainfed area, where a 50 m tower was deployed with sensors at 1.2, 10, 25, and 50 m heights. A full description of the site is given in Brooke et al. (2023). Air temperature, relative humidity, and wind at all heights were measured with Vector Instruments T302, Vaisala HMP155 sensors (both housed in aspirated panels), and Gill HS50 3D ultrasonic anemometers, respectively. Sensible heat and momentum fluxes were measured at all flux tower heights based on 10 Hz data. Latent heat flux was measured at 2 and 10 m with a Krypton hygrometer and a Licor Li-7500 open-path hygrometer, respectively. Canopy measurements included air temperature and relative humidity, measured in situ with a shielded and aspirated Rotronics Hydroclip2 at a nominal height of 8 cm. Radiation measurements are listed in Table 3. Precipitation was measured with a Met Office Mk5 tipping bucket gauge, accurate to 0.2 mm. Subsurface soil moisture and soil temperature were measured, including volumetric soil moisture at five depths (see Table 3). A series of soil evaporation experiments were conducted using a weighable lysimeter (SFL 600, METER). The lysimeter has a dynamic suction-controlled bottom boundary (bi-directional pumping system and weighable drainage tank), which allows the dynamic soil water flow across the lysimeter bottom (inflow and outflow) to match field conditions closely (Groh et al., 2016). Drainage was observed until June 2024 due to severe drought conditions in this region. In addition, the weighing lysimeter provides precise and high temporal resolution measurements to quantify non-rainfall water inputs to this arid ecosystem, such as dew formation (Groh et al., 2018), fog deposition, or the adsorption of water vapor in the soil (Paulus et al., 2024).

2.7.6. Preixana: Almond orchard (Dry Area)

A SEB station was installed in April (with measurements running through October) in a rainfed almond grove (150 × 200 m^2) with a gravel layer covering the soil near Preixana, inside the dry zone. The turbulent fluxes were measured from the top of a scaffold about 2 m above the trees, which were approximately 4 m tall. The system was complemented with soil temperature and moisture measurements buried outside the tree shadows (see Table 3). Four micro-lysimeters were installed to determine the proportion of bare soil in the total ET measured by the eddy covariance system for the almond orchard. In addition, stomatal conductance (SC-1 leaf Porometer, METER) was measured at various points on an almond tree during this 24-hour period.

2.7.7. Verdú: Irrigated vineyard (Dry Area)

A SEB station was installed over a vineyard near the town of Verdú from April 1st to the end of September 2021. The objective of this site was to provide flux, vegetation, and soil moisture measurements for use in an improved version of the Food and Agriculture Organization's Irrigation and Drainage Paper No. 56 (FAO-56) model for row crops (in collaboration with the European Space Agency). Row spacing was 4 m, with no vegetation between the rows. The vineyard is approximately 25 years old. It was originally not irrigated but benefited from the construction of the Segarra-Garrigues canal around 2008, and drip irrigation was installed in 2017. The water emitters are spaced approximately one meter apart at the foot of the vines. The soil is shallow (about 0.50 m) and stony. The instrumentation for measuring turbulent fluxes is listed in Table 3. The fluxes were post-processed by applying instrument-specific corrections and processing commonly used in the scientific literature (filtering, double matrix rotation, Webb term correction, frequency correction). Three Hukseflux soil heat flux plates (two in the row, one in the inter-row at a depth of 5 cm), two SKYE NDVI sensors, three soil moisture sensors in the vegetation row, an SSM sensor in the inter-row area (Mwangi et al., 2023), and one temperature sensor installed in July (see Table 3) were used. Three weather variables were also monitored: rainfall, air temperature, and relative humidity. A weekly field survey of soil moisture and vegetation porosity was also conducted at the site. Five micro-lysimeters were installed to determine the evaporation patterns of the bare soil at different locations between the rows of vines (under the canopy and between the rows) for a full day (24 h) during the SOP. Additionally, stomatal conductance (SC-1, METER) was measured at various points on the vine during this 24-hour period. After gap-filling for relatively small periods, the closure of the SEB was verified. The correlation coefficient was good (0.91); however, the slope was low (0.64). This type of non-closure of the energy budget is common for heterogeneous vegetation, such as that at this site (see, for example, Brunel et al., 2006; Soltani et al., 2018).

2.8. Scintillometers

Scintillometers measure the intensity of optical turbulence along a path between the instrument's transmitter and receiver, typically ranging from approximately 0.1 to 10 km. From these measurements, the spatially averaged fluxes of sensible heat, momentum, water vapor, and CO_2 can be estimated using additional measurements and theoretical assumptions, particularly the validity of Monin–Obukhov similarity theory over the field where they are employed (Ward et al., 2013); (Van Kesteren et al., 2013). This technique is complementary to the traditional eddy covariance method because it can capture fluxes over larger spatial areas and estimate fluxes on shorter time scales (<1 min). Four scintillometers were used during the SOP. Two SLS20 dual-beam laser scintillometers (Scintec AG, Rottenburg, Germany) were installed in parallel at a height of about 2 m along a short 70 m path of the DTS turbulence harp at La Cendrosa. Two combined optical-microwave scintillometer (OMS) systems were deployed over a mixed agricultural area (7.5 m height and 1.3 km path length) in Mollerussa and over Lake Ivars (6.5 m height and 780 m path length) over open water. The OMS systems consisted of a Kipp & Zonen MK-II large aperture optical scintillometer (880 nm wavelength) and a Radiometer Physics GmbH RPG MWSC-160 microwave scintillometer (1.86 mm wavelength). This bichromatic scintillometer system is capable of measuring both sensible and latent heat fluxes.

3. Satellite remote sensing -based s urface d ata over the entire zone

3.1. Irrigation mapping and detection

Maps of irrigation systems are crucial for a better understanding of human impact on the water cycle. At the administrative level, they are a valuable tool for monitoring changes and optimizing irrigation practices. The first level of assessment involved dichotomizing irrigated and non-irrigated areas (Elwan et al., 2022). Different indicators from optical (Sentinel-2) and radar (Sentinel-1) satellite observations, at both low (5 km) and fine (10 m) resolution, were used. A support vector machine classifier, trained on the national agricultural dataset, achieved an overall accuracy of 90.1% and a kappa agreement index of 0.60 for the Urgell region. A second study aimed to classify different irrigation systems at the field level, using remotely sensed data at the sub-field scale as input to various supervised machine learning (ML) models for time series classification (Paolini et al., 2022). The ML models were trained using ground-truth data from over 300 fields collected during a field campaign in 2020 in an intensively cultivated region of Catalunya, Spain. Two hydrological variables retrieved from satellite data, ET and SSM, showed the best results when used for classification, especially when combined. The final classification accuracy was 90.1 ± 2.7%. All three ML models used for classification demonstrated their ability to discriminate between different irrigation systems, regardless of the crops present in each field. In all tests, the best performance was achieved by ResNET, the only deep neural network model among the three tested. The resulting method enables the creation of maps of irrigation systems at the field level and across large areas, providing detailed information on the status and evolution of irrigation practices.

When calculating the water budget of irrigated land, the amount and timing of irrigation are typically simulated according to predetermined decision rules at the plot level. However, actual irrigation events may differ significantly due to farmer or system contingencies. Le Page et al. (2020, 2023) proposed comparing a modeled estimate of soil moisture (SSM) with that estimated from radar satellite observations (El Hajj et al., 2017). A significant divergence between the model and the observation is interpreted as an irrigation event. This technique has shown promising performance in different European countries, with an F-score around 0.6. However, some limitations have been observed, including the accuracy of the SSM estimates from both observations and the model, the masking of the soil by very well-developed vegetation, and the potential mismatch between the frequency of observations and the frequency of irrigation. The algorithm was successfully applied to the Boldu plots. Fig. 9 shows an example for one of the maize plots during the summer of 2021. Of the five irrigation events predicted by the algorithm, one was a false positive, and four were detected with an accuracy of less than 3 days.

3.2. Spatially distributed surface fluxes

Surface flux maps provide estimates of ET and other components of the SEB over large areas and depend, to varying degrees, on remotely sensed data. These maps can be used to characterize the spatial heterogeneity of surface fluxes and properties. Within LIAISE, they will be compared to spatially distributed LSM outputs, which are either forced by reanalysis or coupled to atmospheric models.

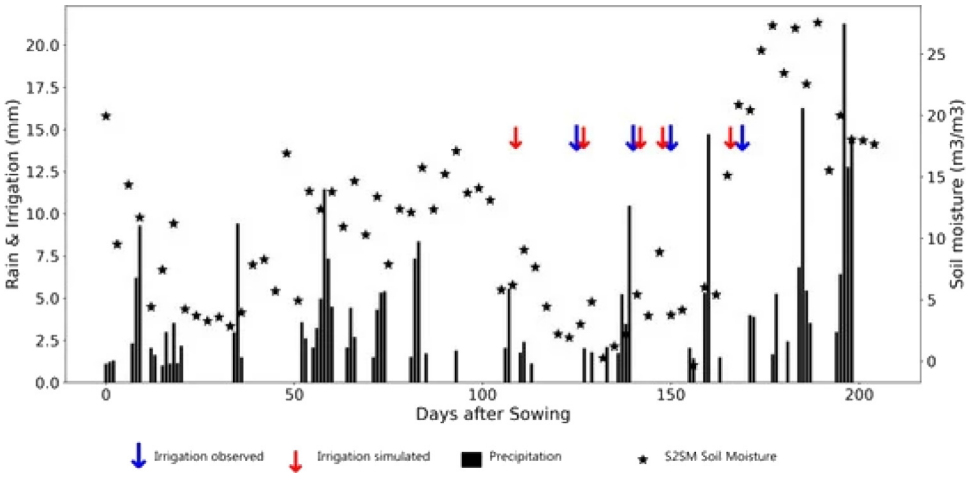

Fig. 9. An example of the irrigation detection algorithm for one of the maize plots at Boldú in summer 2021. S2SM (Sentinel-1 and Sentinel-2 SSM estimates) are shown (as stars). An irrigation event is identified when SSM increases in the absence of significant rainfall. Of the five irrigation events predicted by the algorithm, one was false and four were detected with an accuracy of less than 3 days.

3.2.1. Remote sensing of evapotranspiration

Remotely sensed crop ET was estimated at a 20 m resolution on a daily basis over the entire zone throughout 2021 (an example is shown for July 21 in Fig. 10). The TSEB modeling scheme was used following the methodology described by Guzinski et al. (2020). Vegetation biophysical variables were estimated using the Sentinel-2 biophysical processor available in the Sentinel Application Platform (SNAP) software v8.0 (https://step.esa.int/main/download/snap-download/). This processor is based on the construction of a randomized dataset of vegetation biophysical variables, from which reflectance simulations are generated by the radiative transfer models PROSPECT (leaf reflectance and transmittance) and SAIL (plant canopy reflectance) (Jacquemoud et al., 2009). Therefore, instantaneous values of biophysical variables were obtained at the time of satellite overpass on days with clear sky conditions. Moreover, the LST was retrieved from the Sentinel-3 satellites. A data mining sharpening (DMS) approach was used to sharpen the LST from Sentinel-3, which has a coarse spatial resolution of 1 km, to 20 m (Gao et al., 2012). This approach involves building a regression tree to relate LST to a suite of shortwave spectral reflectance and ancillary data (e.g., elevation, illumination) at a coarse resolution, and then applying it to a fine (shortwave band) pixel resolution. The Priestley-Taylor approach (Priestley and Taylor, 1972) was applied in the TSEB model, which uses an electrical circuit analogy in which H from soil and canopy is estimated based on three aerodynamic resistances to heat transport arranged in a series network (Kustas et al., 2016). Time series analysis of ET was used to quantify crop water requirements at the study site and assess differences in crop water use among crops and irrigation districts. Additionally, further improvements to the modeling approach will be made, mainly focusing on the incorporation of Landsat LST (100 m resolution) into the data fusion methodology and the integration of meteorological variables at higher spatial resolutions generated by the SMC.

3.2.2. Combining land cover and SEB station data to derive flux maps

By combining the data measured at the SEB stations at the seven surface sites during the SOP with a high-resolution land-use map provided by the *Sistema de Información Geográfica de Parcelas Agrícolas* (SIGPAC), the components of the SEB were spatially distributed over the LIAISE domain (Fig. 11). In addition to the observations from the SEB stations, the same approach was applied to ecophysiological observations, such as leaf area index and stomatal conductance, for use in modeling studies. The SIGPAC land-use map was reclassified by crop type to better align with the energy balance stations. According to this land cover database, the LIAISE area consisted of 36% cereals, 21% urban areas, 13% fruit trees, 12.5% corn, and less than 10% each for alfalfa, grass, vineyards, nut trees, and open water. In the absence of observations in urban areas, urban fluxes were modeled using an energy balance closure model described by Román-Cascón et al. (2021) and Mangan et al. (2023). To spatially extrapolate field measurements, it was assumed that the observations from the SEB reference station were representative of all fields of the same crop type in the LIAISE area and that all crops followed the same growing cycle. For more details on the flux maps and crop cover in the LIAISE area, see Section 3.2.2 and Appendix A of Mangan et al. (2023). The flux map data is available in the LIAISE database.

4. Discussion and conclusions

Semi-arid regions are shaped by a complex interplay of natural and anthropogenic processes, so the main objectives of the LIAISE project are to (i) determine what are the key surface processes that modulate or control infiltration and runoff and govern turbulent fluxes and their spatial heterogeneity, (ii) better understand how anthropization impacts ABL development, mesoscale circulations and potentially precipitation recycling over this region via feedbacks with the atmosphere, and (iii) study the sustainability of ground water and reservoirs in the face of expanding agricultural and farming activities, especially in light of projected future warming and drying over this region. To the authors' knowledge, this is the first international project focusing on human impacts on the water and energy cycles in a semi-arid environment, where models are advanced enough to explicitly account for dams, irrigation practices, river flow, groundwater interactions, vegetation phenology, and atmospheric feedback. These models are sophisticated enough to use remote sensing data as input and to employ data assimilation strategies. However, despite recent advances, water management is either overly simplistic or nonexistent in most LSMs. This project seeks to improve the representation of anthropogenic influences in the LSM component of Earth system models. LIAISE addresses how a warming world will affect available freshwater resources globally, especially in food basket regions, and how this will change human interactions with these resources and their value to society. Another key issue addressed by LIAISE is improving our understanding of the impacts and uncertainties of water and energy exchanges in the current and changing climate, as well as how to communicate this information to society. Improving the representation of anthropogenic impacts in models will provide the foundation for studies on the impact of water resources under future climate change. These results are communicated to water management services in the Ebro Basin.

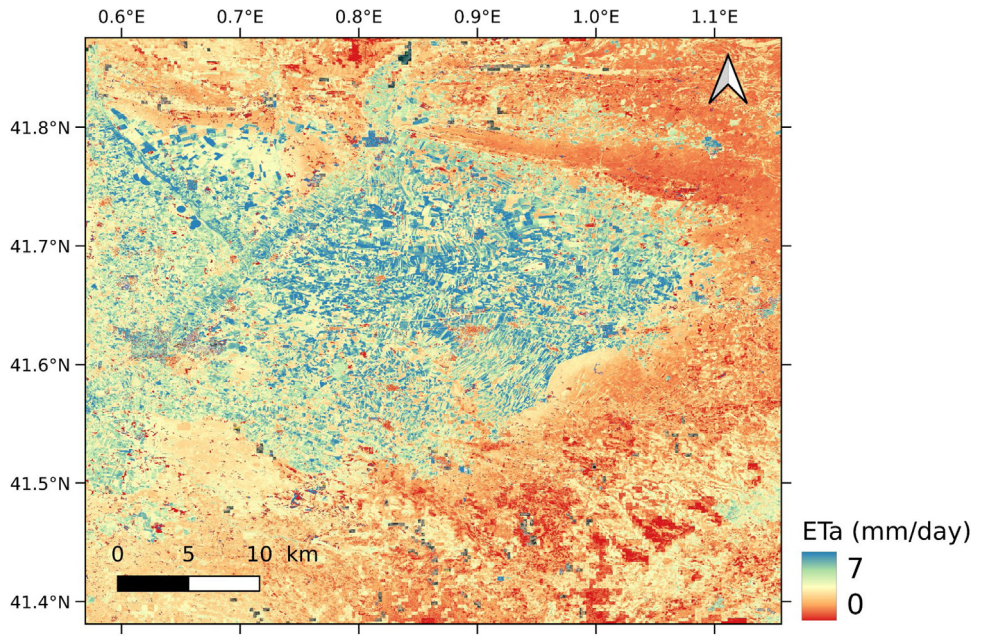

Fig. 10. Actual crop ET image at 20 m resolution during the LIAISE campaign (21 July 2021) estimated using the SEN4ET methodology (https://www.esa-sen4et.org) with Copernicus-based inputs. The methodology used is based on the adoption of the TSEB model with a synergetic use of Sentinel-2 and Sentinel-3 satellite's observations and Copernicus-based inputs.

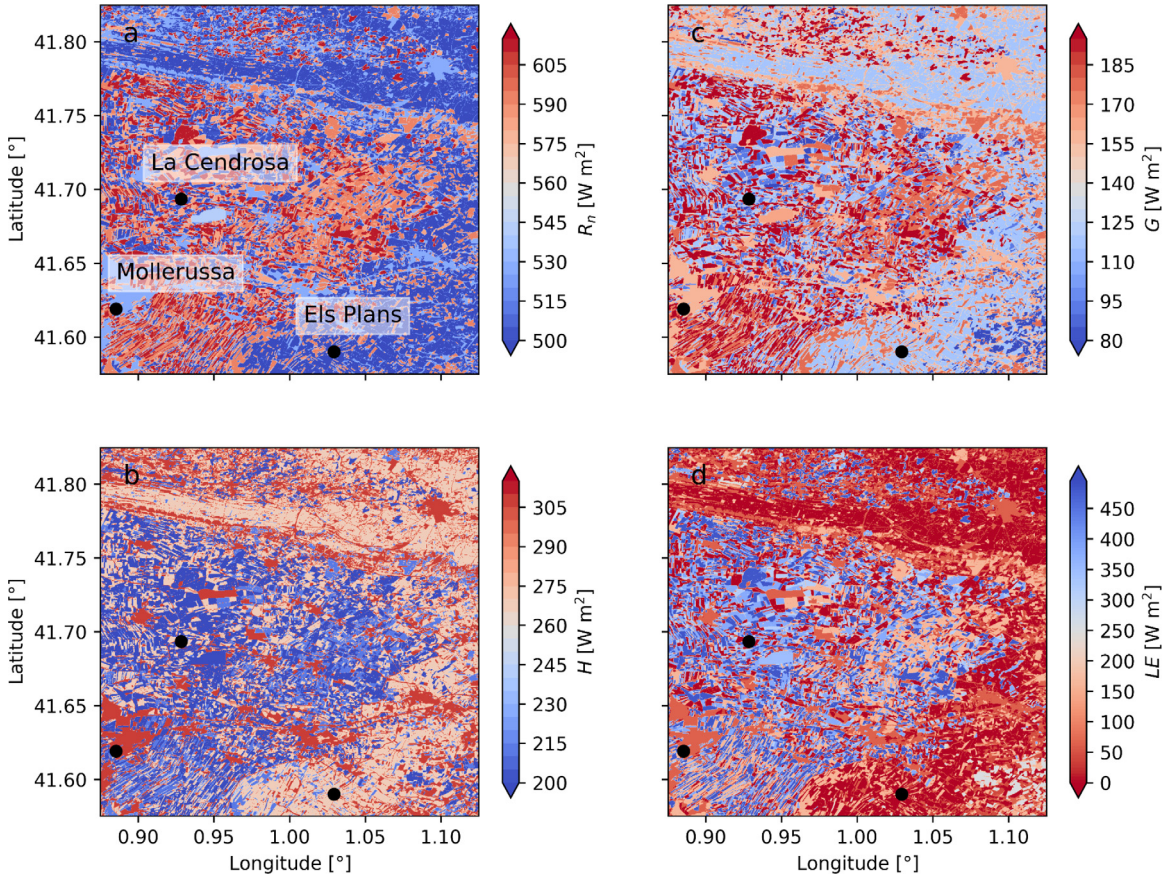

Fig. 11. Surface flux observations which have been upscaled to the LIAISE measurement domain for July 20, 2021 for (a) net radiation, (b) ground heat flux, (c) sensible heat flux, and (d) latent heat flux. The marked sites are the LIAISE "supersites": La Cendrosa alfalfa, Els Plans fallow and Mollerussa mixed agricultural fields.

To attain the goals of the LIAISE project, a field campaign was organized in 2021 which brought together ground-based (surface energy budget estimated at 7 sites, 269 radio soundings made at 2 sites and multiple remote sensing instruments for profiling the lower atmosphere), airborne measurements (3 airplanes and numerous drones measuring surface and atmospheric properties) and satellite data (to

derive estimates of irrigation timing, soil moisture, evapotranspiration and surface temperature) to improve our understanding of key natural and anthropogenic land processes and boundary layer feedbacks. A comprehensive database of surface and airborne measurements of surface and hydrological fluxes, as well as the state and properties of the ABL, has been integrated into the LIAISE database (https://liaise.aeris-data.fr/) and is available upon request to interested researchers.

The LIAISE database is being used in a number of process-based studies to elucidate the key processes driving ET and the interactions between the SEB and the ABL. Currently, the observations are being used to explore land–atmosphere interactions in models using metrics from the GEWEX Local Land–Atmosphere Coupling (LoCo) project. Several studies are studying the impact of irrigation on plant physiological processes, photosynthesis and ET. There is ongoing work using large eddy simulations (LES) forced by surface flux maps (see Section 3.2.2) to study turbulence induced by the surface contrasts using the SOP data. There is also a regional climate model study underway which is studying the impact of the intensively irrigated zone over a larger area covering the entire Iberian peninsula, with the objective of better understanding the overall water budget and whether any of the irrigation water is recycled locally.

This dataset serves as the foundation for several international modeling experiments spanning a wide range of interests. One such project will focus on how land surface models (LSMs) simulate surface processes at the local scale, as presented in Section 2.7. This includes evaluating the ability of LSMs to capture soil moisture drying, represent heterogeneity, and assess the impact of human activities (notably irrigation) on land surface fluxes. In the context of land–atmosphere interactions, a mesoscale inter-model intercomparison study is planned. This study aims to build upon the findings from the modeling efforts of Lunel et al. (2024a,b) and Udina et al. (2024) by employing a multi-model ensemble of kilometer-scale models. These models incorporate varying representations of irrigation, land surface processes, and atmospheric boundary layer (ABL) turbulence. Given that each model's response is shaped by its specific physical parameterizations and input physiographic databases, the study will investigate the impacts of anthropization using this multi-model approach. Ultimately, the goal is for this dataset to support researchers for years to come as they work to deepen our understanding of human impacts on the water and energy cycles. This, in turn, will contribute to better management of precious water resources in the face of climate change.

CRediT authorship contribution statement

Aaron Boone: Writing – original draft, Supervision, Project administration, Methodology, Investigation, Funding acquisition, Conceptualization. **Joaquim Bellvert:** Writing – original draft, Validation, Methodology, Investigation, Funding acquisition, Data curation, Conceptualization. **Martin Best:** Writing – review & editing, Methodology, Investigation, Formal analysis, Conceptualization. **Jennifer K. Brooke:** Writing – original draft, Validation, Methodology, Investigation, Formal analysis, Data curation, Conceptualization. **Guylaine Canut-Rocafort:** Writing – original draft, Validation, Methodology, Investigation, Formal analysis, Data curation, Conceptualization. **Joan Cuxart:** Writing – review & editing, Project administration, Methodology, Investigation, Funding acquisition, Formal analysis, Data curation, Conceptualization. **Oscar Hartogensis:** Writing – original draft, Supervision, Methodology, Investigation, Funding acquisition, Formal analysis, Data curation, Conceptualization. **Patrick Le Moigne:** Writing – review & editing, Investigation, Formal analysis, Conceptualization. **Josep Ramon Miró:** Writing – review & editing, Project administration, Methodology, Investigation, Funding acquisition, Conceptualization. **Jan Polcher:** Project administration, Methodology, Investigation. **Jeremy Price:** Project administration, Methodology, Investigation, Funding acquisition, Formal analysis, Data curation, Conceptualization. **Pere Quintana Seguí:** Project administration, Methodology, Investigation, Funding acquisition. **Joan Bech:** Writing – original draft, Methodology, Investigation, Funding acquisition, Formal analysis, Data curation. **Yannick Bezombes:** Formal analysis, Data curation. **Oliver Branch:** Validation, Investigation, Formal analysis, Data curation. **Jordi Cristóbal:** Writing – original draft, Investigation. **Karin Dassas:** Writing – original draft, Validation, Investigation, Formal analysis, Data curation. **Pascal Fanise:** Investigation, Formal analysis, Data curation. **Fabien Gibert:** Validation, Investigation, Funding acquisition, Formal analysis, Data curation, Conceptualization. **Yves Goulas:** Methodology, Investigation, Formal analysis, Data curation, Conceptualization. **Jannis Groh:** Writing – review & editing, Investigation, Formal analysis, Data curation. **Jan Hanus:** Writing – original draft, Methodology, Investigation, Funding acquisition, Formal analysis, Data curation. **Gabriel Hmimina:** Investigation, Formal analysis. **Lionel Jarlan:** Project administration, Methodology, Investigation, Conceptualization. **Ed Kim:** Writing – original draft, Methodology, Investigation, Funding acquisition, Formal analysis, Data curation, Conceptualization. **Valérie Le Dantec:** Writing – original draft, Methodology, Investigation, Formal analysis, Data curation. **Michel Le Page:** Methodology, Investigation, Formal analysis, Data curation. **Fabienne Lohou:** Methodology, Investigation, Formal analysis, Data curation. **Marie Lothon:** Writing – original draft, Methodology, Investigation, Formal analysis, Data curation, Conceptualization. **Mary Rose Mangan:** Writing – original draft, Investigation, Formal analysis, Data curation. **Belén Martí:** Writing – review & editing, Investigation, Formal analysis, Data curation. **Daniel Martínez-Villagrasa:** Writing – original draft, Methodology, Investigation, Funding acquisition, Formal analysis, Data curation. **James McGregor:** Investigation, Formal analysis, Data curation. **Amanda Kerr-Munslow:** Formal analysis, Data curation. **Nadia Ouaadi:** Writing – original draft, Methodology, Investigation, Formal analysis, Data curation. **Alban Philibert:** Investigation, Formal analysis, Data curation. **Juan Quiros-Vargas:** Investigation, Formal analysis, Data curation. **Uwe Rascher:** Project administration, Methodology, Investigation, Data curation, Conceptualization. **Bastian Siegmann:** Writing – original draft, Methodology, Investigation, Formal analysis, Data curation. **Mireia Udina:** Investigation, Formal analysis. **Antoine Vial:** Formal analysis, Data curation. **Burkhard Wrenger:** Writing – original draft, Methodology, Investigation, Formal analysis, Data curation. **Volker Wulfmeyer:** Methodology, Investigation, Funding acquisition. **Mehrez Zribi:** Methodology, Investigation, Formal analysis, Data curation.

Declaration of competing interest

The authors declare the following financial interests/personal relationships which may be considered as potential competing interests: Aaron Boone reports financial support was provided by French National Research Agency. If there are other authors, they declare that they have no known competing financial interests or personal relationships that could have appeared to influence the work reported in this paper.

Acknowledgments

We wish to acknowledge the financial support of the French National Agency for research (grant number ANR-19-CE01-0017 in support of the project ''HILIAISE : Human imprint on Land surface Interactions with the Atmosphere over the Iberian Semi-arid Environment'') which funded the ATR42 flights, field work by numerous French laboratories and overall project support. The Service des Avions Français Instrumentés pour la Recherche en Environnement (SAFIRE) team is also acknowledged for the excellent execution of the air campaign. J. Cuxart, D. Martínez-Villagrasa, B. Martí, J.R. Miró and Burkhard Wrenger acknowledge projects WISE-ET (RTI2018-098693-B-C31) and WET-ARID (PID2021-124006OB-I00) funded by Spanish MCIN/AEI/10.13039/501100011033 and by the European Regional Development Fund (ERDF A way of making Europe). J. Groh is funded

by the Deutsche Forschungsgemeinschaft (DFG, German Research Foundation) - project no. 460817082. J. Bellvert and J. Cristóbal acknowledge the support by the Project ET4DROUGHT (No. PID2021-127345OR-C31) funded by the Ministry of Science and Innovation (MICINN-AEI) of Spain and PRIMA ALTOS [No. PCI 2019–103649]. M. Le Page and P. Fanise acknowledge the support by project WINEO funded by the European Space Agency. A. Rouchon acknowledges funding from École Nationale de la Météorologie, Météo-France. B. Martí was supported during the campaign by the grant FPI-CAIB (FPI/2165/2018) of the *Vicepresidència i Conselleria d'Innovació, Recerca i Turisme del Govern de les Illes Balears* and the *Fons Social Europeu* (European Social Fund). We gratefully acknowledge the financial support of the European Space Agency (ESA) for developing the HyPlant processing pipeline in the frame of the FLEXSense campaign (ESA Contract No. 4000125402/18/NL/NA) and the Photoproxy project (ESA contract No. 4000125731/19/NL/LF). Additionally, we want to acknowledge the financial support by the 'Strukturwandel-Projekt Bioökonomie REVIER', which is funded by the German Federal Ministry of Education and Research (project identification number 031B0918A) and the Deutsche Forschungsgemeinschaft (DFG, German Research Foundation) under Germany Excellence Strategy – EXC 2070–390732324. The authors would like to acknowledge the Observation-based Research Boundary Layer Measurement Facility staff at the Met Office including Tony Jones, Robert Clark, Martyn Pickering, Bernard Claxton, and Jenna Thorton. The authors are very grateful to local actors for their support: Josep Berenguer and the ensemble of the involved IRTA personnel, Carme Bernat of Canal Segarra-Garrigues and the team of SAF-sampling at Els Plans site, the Catalan Firefighters of the Catalan Government for their help with the setting of the scintillometers, the Pla d'Urgell county for the access to the Ivars-Vilasana Lake, and Josep Maria Tribó for allowing the use of the alfalfa field at La Cendrosa. We wish to thank the Ajuntament de Preixana for their assistance in hosting a measurement site. M. Udina and J. Bech acknowledge support from the Water Research Institute of the University of Barcelona, and the Spanish projects MCIN/AEI/10.13039/501100011033 (PID2021-124253OB-I00 ARTEMIS and RTI2018-098693-B-C32 WISE-PreP). Finally, we wish to thank the AERIS data center for hosting and providing user support of the LIAISE database (https://liaise.aeris-data.fr/). The LIAISE project webpage is supported by Météo-France and can be accessed at https://www.hymex.fr/liaise/.

Data availability

Data will be made available on request.

References

Agam, N., Evett, S.R., Tolk, J.A., Kustas, W.P., Colaizzi, P.D., Alfieri, J.G., McKee, L.G., Copeland, K.S., Howell, T.A., Chávez, J.L., 2012. Evaporative loss from irrigated interrows in a highly advective semi-arid agricultural area. Adv. Water Resour. 50, 20–30. http://dx.doi.org/10.1016/j.advwatres.2012.07.010.

Alter, R.E., Im, E.-S., Eltahir, E.A.B., 2015. Rainfall consistently enhanced around the Gezira Scheme in East Africa due to irrigation. Nat. Geosci. 8, 763–767. http://dx.doi.org/10.1038/ngeo2514.

Aouade, G., Ezzahar, J., Amenzou, N., Er-Raki, S., Benkaddour, A., Khabba, S., Jarlan, L., 2016. Combining stable isotopes, eddy covariance system and meteorological measurements for partitioning evapotranspiration, of winter wheat, into soil evaporation and plant transpiration in a semi-arid region. Agric. Water Manag. 177, 181–192. http://dx.doi.org/10.1016/j.agwat.2016.07.021.

Bech, J., Garcia-Benadí, A., Udina, M., Polls, M., Peinó, E., Balagué, M., Paci, A., Boudevillain, B., 2024. Analysis of rainfall characteristics and evaporation processes using vertically pointing doppler radars during the LIAISE field campaign. In: 104th AMS Annual Meeting, Baltimore, USA.

Bellvert, J., Pamies-Sans, M., Quintana-Segui, P., Casadesús, J., 2024. Analysis and forecast of crop water demand in irrigation districts across the eastern part of the Ebro river basin (Catalonia, Spain): estimation of evapotranspiration through copernicus-based inputs. Irrig. Sci. http://dx.doi.org/10.1007/s00271-024-00971-1.

Bolle, H.J., 1995. Identification and observation of desertification processes with the aid of measurements from space: Results from the European field experiment in desertification-threatened areas (EFEDA). Environ. Monit. Assess. 37, 93–101. http://dx.doi.org/10.1007/BF00546882.

Bony, S., Lothon, M., Delanoë, J., Coutris, P., Etienne, J.-C., Aemisegger, F., Albright, A.L., André, T., Bellec, H., Baron, A., Bourdinot, J.-F., Brilouet, P.-E., Bourdon, A., Canonici, J.-C., Caudoux, C., Chazette, P., Cluzeau, M., Cornet, C., Desbios, J.-P., Duchanoy, D., Flamant, C., Fildier, B., Gourbeyre, C., Guiraud, L., Jiang, T., Lainard, C., Gac, C.Le., Lendroit, C., Lernould, J., Perrin, T., Pouvesle, F., Richard, P., Rochetin, N., Salaün, K., Schwarzenboeck, A., Seurat, G., Stevens, B., Totems, J., Touzé-Peiffer, L., Vergez, G., Vial, J., Villiger, L., Vogel, R., 2022. EUREC^{4}A observations from the SAFIRE ATR42 aircraft. Earth Syst. Sci. Data 14, 2021–2064. http://dx.doi.org/10.5194/essd-14-2021-2022.

Brilouet, P.-E., Lothon, M., Etienne, J.-C., Richard, P., Bony, S., Lernoult, J., Bellec, H., Vergez, G., Perrin, T., Delanoë, J., Jiang, T., Pouvesle, F., Lainard, C., Cluzeau, M., Guiraud, L., Medina, P., Charoy, T., 2021. The EUREC4A turbulence dataset derived from the SAFIRE ATR 42 aircraft. Earth Syst. Sci. Data 13, 3379–3398. http://dx.doi.org/10.5194/essd-13-3379-2021.

Brooke, J.K., Best, M.J., Lock, A.P., Osborne, S.R., Price, J., Cuxart, J., Hartogensis, O., Boone, A., Roy, A., 2023. Irrigation contrasts through the morning transition. Q. J. R. Meteorol. Soc. 150, 170–194. http://dx.doi.org/10.1002/qj.4590.

Brunel, J.-P., Ihab, J., Droubi, A.M., Samaan, S., 2006. Energy budget and actual evapotranspiration of an arid oasis ecosystem: Palmyra (Syria). Agric. Water Manag. 84 (3), 213–220. http://dx.doi.org/10.1016/j.agwat.2006.02.005.

Cammalleri, C., Rallo, G., Agnese, C., Ciraolo, G., Minacapilli, M., Provenzano, G., 2013. Combined use of eddy covariance and sap flow techniques for partition of ET fluxes and water stress assessment in an irrigated olive orchard. Agric. Water Manag. 120, 89–97. http://dx.doi.org/10.1016/j.agwat.2012.10.003.

Cogliati, S., Celesti, M., Cesana, I., Miglietta, F., Genesio, L., Julitta, T., Schuettemeyer, D., Drusch, M., Rascher, U., Jurado, P., Colombo, R., 2019. A spectral fitting algorithm to retrieve the fluorescence spectrum from canopy radiance. Remote Sens. 11 (1840), http://dx.doi.org/10.3390/rs11161840.

Cos, J., Doblas-Reyes, F., Jury, M., Marcos, R., Bretonnière, P.-A., Samsó, M., 2022. The Mediterranean climate change hotspot in the CMIP5 and CMIP6 projections. Earth Syst. Dynam. 13, 321–340. http://dx.doi.org/10.5194/esd-13-321-2022.

Courtier, P., Thépaut, J.-N., Hollingsworth, A., 1994. A strategy for operational implementation of 4D-VAR using an incremental approach. Q. J. R. Meteorol. Soc. 120, 1367–1387. http://dx.doi.org/10.1002/qj.49712051912.

Cuxart, J., Boone, A., 2020. Evapotranspiration over land from a boundary-layer meteorology perspective. Bound.-Layer Meteorol. 177, 427–459. http://dx.doi.org/10.1007/s10546-020-00550-9.

Cuxart, J., Cunillera, J., Jiménez, M.A., Martínez, D., Molinos, F., Palau, J.L., 2012. Study of mesobeta basin flows by remote sensing. Bound.-Layer Meteorol. 143, 143–158. http://dx.doi.org/10.1007/s10546-011-9655-8.

Cuxart, J., Verhoef, A., Marthews, T.R., Evans, J., 2019. Current challenges in evapotranspiration determination. GEWEX News 29 (1), 5–8, https://www.gewex.org/gewex-content/uploads/2024/02/1551991026Q1_2019.pdf.

Dassas, K., Fanise, P., Le Page, M., Ayari, E., Baillion, P., Sige, M., Boone, A., Zribi, M., 2024. Polarimetric instrument global navigation satellite system-reflectometry airborne data. Data Brief 52, 109850. http://dx.doi.org/10.1016/j.dib.2023.109850.

Diffenbaugh, N.S., Giorgi, F., 2012. Climate change hotspots in the CMIP5 global climate model ensemble. Clim. Change 114, 813–822. http://dx.doi.org/10.1007/s10584-012-0570-x.

Drobinski, P., Ducrocq, V., Alpert, P., Anagnostou, E., Béranger, K., Borga, M., Braud, I., Chanzy, A., Davolio, S., Delrieu, G., Estournel, C., Boubrahmi, N.Filali., Font, J., Grubišić, V., Gualdi, S., Homar, V., Ivančan-Picek, B., Kottmeier, C., Kotroni, V., Lagouvardos, K., Lionello, P., Llasat, M.C., Ludwig, W., Lutoff, C., Mariotti, A., Richard, E., Romero, R., Rotunno, R., Roussot, O., Ruin, I., Somot, S., Taupier-Letage, I., Tintore, J., Uijlenhoet, R., Wernli, H., 2014. HyMeX: A 10-year multidisciplinary program on the Mediterranean water cycle. Bull. Am. Meterol. Soc. 95, 1063–1082. http://dx.doi.org/10.1175/BAMS-D-12-00242.1.

Dyer, A.J., Hicks, B.B., 1970. Flux-gradient relationships in the constant flux layer. Q. J. R. Meteorol. Soc. 96, 715–721. http://dx.doi.org/10.1002/qj.49709641012.

El Hajj, M., Baghdadi, N., Zribi, M., Bazzi, H., 2017. Synergic use of sentinel-1 and sentinel-2 images for operational soil moisture mapping at high spatial resolution over agricultural areas. Remote Sens. 9 (1292), http://dx.doi.org/10.3390/rs9121292.

Elwan, E., Le Page, M., Jarlan, L., Baghdadi, N., Brocca, L., Modanesi, S., Dari, J., Segui, P.Quintana., Zribi, M., 2022. Irrigation mapping on two contrasted climatic contexts using sentinel-1 and sentinel-2 data. Water 14 (804), http://dx.doi.org/10.3390/w14050804.

Evett, S.R., Kustas, W.P., Gowda, P.H., Anderson, M.C., Prueger, J.H., Howell, T.A., 2012. Overview of the bushland evapotranspiration and agricultural remote sensing experiment 2008 (BEAREX08): A field experiment evaluating methods for quantifying ET at multiple scales. Adv. Water Resour. 50, 4–19. http://dx.doi.org/10.1016/j.advwatres.2012.03.010.

Eyring, V., Bony, S., Meehl, G.A., Senior, C.A., Stevens, B., Stouffer, R.J., Taylor, K.E., 2016. Overview of the coupled model intercomparison project phase 6 (CMIP6) experimental design and organization. Geosci. Model Dev. 9, 1937–1958. http://dx.doi.org/10.5194/gmd-9-1937-2016.

Fratini, G., Mauder, M., 2014. Towards a consistent eddy-covariance processing: an intercomparison of EddyPro and TK3. Atmos. Meas. Tech. 7, 2273–2281. http://dx.doi.org/10.5194/amt-7-2273-2014.

Gao, F., Kustas, W.P., Anderson, M.C., 2012. A data mining approach for sharpening thermal satellite imagery over land. Remote Sens. 4, 3287–3319. http://dx.doi.org/10.3390/rs4113287.

Goodrich, D.C., Chehbouni, A., Goff, B., MacNish, B., Maddock, T., Moran, S., Shuttleworth, W.J., Williams, D.G., Watts, C., Hipps, L.H., Cooper, D.I., Schieldge, J., Kerr, Y.H., Arias, H., Kirkland, M., Carlos, R., Cayrol, P., Kepner, W., Jones, B., Avissar, R., Begue, A., Bonnefond, J.-M., Boulet, G., Branan, B., Brunel, J.P., Chen, L.C., Clarke, T., Davis, M.R., DeBruin, H., Dedieu, G., Elguero, E., Eichinger, W.E., Everitt, J., Garatuza-Payan, J., Gempko, V.L., Gupta, H., Harlow, C., Hartogensis, O., Helfert, M., Holifield, C., Hymer, D., Kahle, A., Keefer, T., Krishnamoorthy, S., Lhomme, J.-P., Lagouarde, J.-P., Seen, D.Lo., Luquet, D., Marsett, R., Monteny, B., Ni, W., Nouvellon, Y., Pinker, R., Peters, C., Pool, D., Qi, J., Rambal, S., Rodriguez, J., Santiago, F., Sano, E., Schaeffer, S.M., Schulte, M., Scott, R., Shao, X., Snyder, K.A., Sorooshian, S., Unkrich, C.L., Whitaker, M., Yucel, I., 2000. Preface paper to the semi-arid land-surface-atmosphere (SALSA) program special issue. Agric. Forest Meteorol. 105, 3–20. http://dx.doi.org/10.1016/S0168-1923(00)00178-7.

Goutorbe, J.P., Lebel, T., Dolman, A.J., Gash, J.H.C., Kabat, P., Kerr, Y.H., Monteny, B., Prince, S.D., Stricker, J.N.M., Tinga, A., Wallace, J.S., 1997. An overview of HAPEX-Sahel: a study in climate and desertification. J. Hydrol. 188, 4–17. http://dx.doi.org/10.1016/S0022-1694(96)03308-2.

Groh, J., Slawitsch, V., Herndl, M., Graf, A., Vereecken, H., Pütz, T., 2018. Determining dew and hoar frost formation for a low mountain range and alpine grassland site by weighable lysimeter. J. Hydrol. 563, 372–381. http://dx.doi.org/10.1016/j.jhydrol.2018.06.009.

Groh, J., Vanderborght, J., Pütz, T., Vereecken, H., 2016. How to control the lysimeter bottom boundary to investigate the effect of climate change on soil processes?. Vadose Zone J. 15, 1–25. http://dx.doi.org/10.2136/vzj2015.08.0113.

Guzinski, R., Nieto, H., Sandholt, I., Karamitilios, G., 2020. Modelling high-resolution actual evapotranspiration through sentinel-2 and sentinel-3 data fusion. Remote Sens. 12 (1433), http://dx.doi.org/10.3390/rs12091433.

Harding, R., Polcher, J., Boone, A., Ek, M., Wheater, H., Nazemi, A., 2015. Anthropogenic influences on the global water cycle - challenges for the GEWEX community. GEWEX Q. 27 (4), 6–8.

Hirschi, M., Dominik Michel, M., Lehner, I., Seneviratne, S.I., 2017. A site-level comparison of lysimeter and eddy covariance flux measurements of evapotranspiration. Hydrol. Earth Syst. Sci. 21, 1809–1825. http://dx.doi.org/10.5194/hess-21-1809-2017.

Huang, Y., Meng, Z., Li, W., Bai, L., Meng, X., 2019. General features of radar-observed boundary layer convergence lines and their associated convection over a sharp vegetation-contrast area. Geophys. Res. Lett. 46, 2865–2873. http://dx.doi.org/10.1029/2018GL081714.

Jacoby-Koaly, S., Campistron, B., Bernard, S., Bénech, B., Ardhuin-Girard, F., Dessens, J., Dupont, E., Carissimo, B., 2002. Turbulent dissipation rate in the boundary layer via UHF wind profiler Doppler spectral width measurements. Bound.-Layer Meteorol. 103, 361–389. http://dx.doi.org/10.1023/A:1014985111855.

Jacquemoud, S., Verhoef, W., Baret, F., Bacour, C., Zarco-Tejada, P.J., Asner, G.P., François, C., Ustin, S.L., 2009. PROSPECT+SAIL models: A review of use for vegetation characterization. Remote Sens. Environ. 113, 56–66. http://dx.doi.org/10.1016/j.rse.2008.01.026.

Jiminéz Cortéz, M.A., Grau, A., Martínez-Villagrasa, D., Cuxart, J., 2023. Characterization of the marine-air intrusion Marinada in the eastern Ebro sub-basin. Int. J. Climatol. 43, 7682–7699. http://dx.doi.org/10.1002/joc.8287.

Kim, E., Wu, A., Izadkhah, H., Abraham, S., 2023. High-resolution soil moisture-a European airborne campaign using NASA goddard's scanning L-Band active passive (SLAP). Remote. Sens. Earth Syst. Sci. 6, 309–321. http://dx.doi.org/10.1007/s41976-023-00099-4.

Kustas, W.P., Anderson, M.C., Alfieri, J.G., Knipper, K., Torres-Rua, A., Parry, C.K., Nieto, H., Agam, N., White, W.A., Gao, F., McKee, L., Prueger, J.H., Hipps, L.E., Los, S., Mar Alsina, M., Sanchez, L., Sams, B., Dokoozlian, N., McKee, M., Jones, S., Yang, Y., Wilson, T.G., Lei, F., McElrone, A., Heitman, J.L., Howard, A.M., Post, K., Melton, F., Hain, C., 2018. The grape remote sensing atmospheric profile and evapotranspiration experiment. Bull. Am. Meterol. Soc. 99, 1791–1812. http://dx.doi.org/10.1175/BAMS-D-16-0244.1.

Kustas, W.P., Nieto, H., Morillas, L., Anderson, M.C., Alfieri, J.G., Hipps, L.E., Villagarcía, L., Domingo, F., García, M., 2016. Revisiting the paper using radiometric surface temperature for surface energy flux estimation in Mediterranean drylands from a two-source perspective. Remote Sens. Environ. 184, 645–653. http://dx.doi.org/10.1016/J.RSE.2016.07.024.

Lawston, P.M., Santanello, Jr., J.A., Hanson, B., Arsensault, K., 2020. Impacts of irrigation on summertime temperatures in the Pacific northwest. Earth Interact. 24, 1–16. http://dx.doi.org/10.1175/EI-D-19-0015.1.

Le Page, M., Jarlan, L., Hajj, M.El., Zribi, M., Baghdadi, N., Boone, A., 2020. Potential for the detection of irrigation events on maize plots using sentinel-1 soil moisture products. Remote Sens. 12 (1621), http://dx.doi.org/10.3390/rs12101621.

Le Page, M., Nguyen, T., Zribi, M., Boone, A., Dari, J., Modanesi, S., Zappa, L., Ouaadi, N., Jarlan, L., 2023. Irrigation timing retrieval at the plot scale using surface soil moisture derived from sentinel time series in Europe. Remote Sens. 15 (1449), http://dx.doi.org/10.3390/rs15051449.

Legain, D., Bousquet, O., Douffet, T., Tzanos, D., Moulin, E., Barrie, J., Renard, J.-B., 2013. High-frequency boundary layer profiling with reusable radiosondes. Atmos. Meas. Tech. 6, 2195–2205. http://dx.doi.org/10.5194/amt-6-2195-2013.

Lo, M.-H., Famiglietti, J.S., 2013. Irrigation in California's central valley strengthens the southwestern U.S. water cycle. Geophys. Res. Lett. 40, 301–306. http://dx.doi.org/10.1002/grl.50108.

Lunel, T., Boone, A., Le Moigne, P., 2024a. Influence of irrigation on near-surface conditions and breeze circulation: Evidence from observations and models. Q. J. R. Meteorol. Soc. http://dx.doi.org/10.1002/qj.4736.

Lunel, T., Jiménez, M.A., Cuxart, J., Martinez-Villagrasa, D., Boone, A., Le Moigne, P., 2024b. The Marinada fall wind in the eastern Ebro sub-basin: Physical mechanisms and role of the sea, orography and irrigation. Atmos. Chem. Phys. http://dx.doi.org/10.5194/egusphere-2024-495.

Mahrt, L., Sun, J., Vickers, D., McPherson, J.I., Pederson, J.R., Desjardins, R.L., 1994. Observations of fluxes and inland breezes over a heterogeneous surface. J. Atmos. Sci. 51, 2484–2499. http://dx.doi.org/10.1175/1520-0469(1994)051%E2%9F%A82484:OOFAIB%E2%9F%A92.0.CO;2.

Mangan, M.R., Hartogensis, O., Boone, A., Branch, O., Canut, G., Cuxart, J., de Boer, H., Le Page, M., Martínez-Villagrasa, D., Ramon Miró, J., Price, J., Vilà-Guerau de Arellano, J., 2023. The surface-boundary layer connection across spatial scales of irrigation-driven thermal heterogeneity: An integrated data and modeling study of the LIAISE field campaign. Agric. Forest Meteorol. 335, 109452. http://dx.doi.org/10.1016/j.agrformet.2023.109452.

Martí, B., Martínez-Villagrasa, D., Cuxart, J., 2022. Flux-gradient relationships below 2 m over a flat site in complex terrain. Bound.-Layer Meteorol. 184, 505–530. http://dx.doi.org/10.1007/s10546-022-00719-4.

Massman, W., 2000. A simple method for estimating frequency response corrections for eddy covariance systems. Agricult. Forest. Meterol. 104, 185–198. http://dx.doi.org/10.1016/S0168-1923(00)00164-7.

Mauder, M., Foken, T., 2004. Documentation and Instruction Manual of the Eddy Covariance Software Package TK2 Arbeitsergebn, vol. 26, (42), University of Bayreuth, Abt. Mikrometeorolgy, Available at: https://epub.uni-bayreuth.de/2130/1/ARBERG062.pdf. (Last Access:2020).

Mercader, J., Codina, B., Sairouni, A., Cunillera, J., 2010. Results of the meteorological model WRF-ARW over catalonia, using different parameterizations of convection and cloud microphysics. J. Weather Clim. West. Mediterr. 7, 75–86. http://dx.doi.org/10.3369/tethys.2010.7.07.

Moncrieff, J., Clement, R., Finnigan, J., Meyers, T., 2004. Averaging, detrending, and filtering of eddy covariance time series. In: Lee, X., Massman, W., Law, B. (Eds.), In: Handbook of Micrometeorology, vol. 29, Springer, Dordrecht, http://dx.doi.org/10.1007/1-4020-2265-4_2.

Mwangi, S., Boulet, G., Le Page, M., Gastellu-Etchegorry, J.-P., Bellvert, J., Lemaire, B., Fanise, P., Roujean, J.-L., Olioso, A., 2023. Observation and assessment of model retrievals of surface exchange components over a row canopy using directional thermal data. IEEE J. Sel. Top. Appl. Earth Obs. Remote. Sens. 16, 7343–7356. http://dx.doi.org/10.1109/JSTARS.2023.3297709.

Ouaadi, N., Jarlan, L., Le Page, M., Zribi, M., Paolini, G., Ait Hssaine, B., Escorihuela, M.J., Fanise, P., Merlin, O., N. Baghdadi, N., Boone, A., 2024. Inter-comparison of high-resolution surface soil moisture products over Spain. Remote Sens. Environ. 309, 114225. http://dx.doi.org/10.1016/j.rse.2024.114225.

Paolini, G., Escorihuela, M.J., Merlin, O., Sans, M.P., Bellvert, J., 2022. Classification of different irrigation systems at field scale using time-series of remote sensing data. IEEE J. Sel. Top. Appl. Earth Obs. Remote. Sens. 15, 10055–10072. http://dx.doi.org/10.1109/JSTARS.2022.3222884.

Paulus, S.J., Orth, R., Lee, S.-C., Hildebrandt, A., Jung, M., Nelson, J.A., El-Madany, T.S., Carrara, A., Moreno, G., Mauder, M., Groh, J., Graf, A., Reichstein, M., Migliavacca, M., 2024. Interpretability of negative latent heat fluxes from eddy covariance measurements in dry conditions. Biogeosciences 21, 2051–2085. http://dx.doi.org/10.5194/bg-21-2051-2024.

Philibert, A., Lothon, M., Amestoy, J., Meslin, P.-Y., Derrien, S., Bezombes, Y., Campistron, B., Lohou, F., Vial, A., Canut-Rocafort, G., Reuder, J., Brooke, J.K., 2024. CALOTRITON: a convective boundary layer height estimation algorithm from ultra-high-frequency (UHF) wind profiler data. Atmos. Meas. Tech. 6, 1679–1701. http://dx.doi.org/10.5194/amt-17-1679-2024.

Phillips, C.E., Nair, U.S., Mahmood, R., Rappin, E., Pielke, R.A., 2022. Influence of irrigation on diurnal mesoscale circulations: Results from GRAINEX. Geophys. Res. Lett. 49, 1–12. http://dx.doi.org/10.1029/2021gl096822.

Pielke, Sr., R.A., 2001. Influence of the spatial distribution of vegetation and soils on the prediction of cumulus convective rainfall. Rev. Geophys. 39, 151–177. http://dx.doi.org/10.1029/1999RG000072.

Polls, F., Peinó, E., Udina, M., Bech, J., 2024. Analysis of potential evaporation effects on C-band weather radar rainfall observations in a semi-arid area. In: 12th European conference on Radar in Meteorology and Hydrology, Rome, Italy.

Pörtner, H.-O., Roberts, D.C., Poloczanska, E.S., Mintenbeck, K., Tignor, M., Alegría, A., Craig, M., Langsdorf, S., Löschke, S., Möller, V., Okem, A., 2022. Climate change 2022: impacts, adaptation and vulnerability. In: Contribution of WGII to the AR6 of the IPCC: Summary for Policymakers. 2022. http://dx.doi.org/10.1017/9781009325844.001.

Priestley, C.H.B., Taylor, R.J., 1972. On the assessment of surface heat flux and evaporation using large-scale parameters. Mon. Weather Rev. 100, 81–92. http://dx.doi.org/10.1175/1520-0493(1972)100<0081:OTAOSH>2.3.CO;2.

Quade, M., Klosterhalfen, A., Graf, A., Brüggemann, N., Hermes, N., Vereecken, H., Rothfuss, Y., 2019. In-situ monitoring of soil water isotopic composition for partitioning of evapotranspiration during one growing season of sugar beet (Beta vulgaris). Agric. Forest Meteorol. 266–267, 53–64. http://dx.doi.org/10.1016/j.agrformet.2018.12.002.

Rafi, Z., Merlin, O., Le Dantec, V., Khabba, S., Mordelet, P., Er-Raki, S., Amazirh, A., Olivera-Guerra, L., Ait Hssaine, B., Simonneaux, V., Ezzahar, J., Ferrer, F., 2019. Partitioning evapotranspiration of a drip-irrigated wheat crop: Inter-comparing eddy covariance-, sap flow, lysimeter and FAO-based methods. Agricult. Forest Meteorol. 265, 310–326. http://dx.doi.org/10.1016/j.agrformet.2018.11.031.

Rappin, E., Mahmood, R., Nair, U., Pielke, Sr., R.A., Brown, W., Oncley, S., Wurman, J., Kosiba, K., Kaulfus, A., Phillips, C., Lachenmeier, E., Santanello, Jr., J., Kim, E., Lawston-Parker, P., 2021. The great plains irrigation experiment (GRAINEX). Bull. Am. Meterol. Soc. 102, 1757–1785. http://dx.doi.org/10.1175/BAMS-D-20-0041.1.

Rascher, U., Alonso, L., Burkhart, A., Cilia, C., Cogliati, S., Colombo, R., Damm, A., Drusch, M., Guanter, L., Hanus, J., Hyvarinen, T., Julitta, T., Jussila, J., Katajak, K., Kokkalis, P., Kraft, S., Kraska, T., Matveeva, M., Moreno, J., Muller, O., Panigada, C., Pikl, M., Pinto, F., Prey, L., Pude, R., Rossini, M., Schickling, A., Schurr, U., Schüttemeyer, D., Verrelst, J., Zemek, F., 2015. Sun-induced fluorescence - a new probe of photosynthesis: first maps from the imaging spectrometer hyplant. Glob. Change Biol. 21, 4673–4684. http://dx.doi.org/10.1111/gcb.13017.

Ricart, S., Ribas, A., Pavón, D., 2016. Qualifying irrigation system sustainability by means of stakeholder perceptions and concerns: lessons from the Segarra-Garrigues Canal, Spain. In: Natural Resources Forum, vol. 40, (1-2), Blackwell Publishing Ltd, Oxford, UK, pp. 77–90.

Román-Cascón, C., Lothon, M., Lohou, F., Hartogensis, O., Vila-Guerau de Arellano, J., Pino, D., Yagüe, C., Pardyjak, E.R., 2021. Surface representation impacts on turbulent heat fluxes in the weather research and forecasting (WRF) model (v.4.1.3). Geosci. Model Dev. 14, 3939–3967. http://dx.doi.org/10.5194/gmd-14-3939-2021.

Saïd, F., Canut, G., Durand, P., Lohou, F., Lothon, M., 2010. Seasonal evolution of boundary-layer turbulence measured by aircraft during the AMMA 2006 special observation period. Q. J. R. Meteorol. Soc. 136, 47–65. http://dx.doi.org/10.1002/qj.475.

Seity, Y., Brousseau, P., Malardel, S., Hello, G., Bénard, P., Bouttier, F., Lac, C., Masson, V., 2011. The AROME-France convective-scale operational model. Mon. Weather Rev. 139, 976–991. http://dx.doi.org/10.1175/2010MWR3425.1.

Siegmann, B., Alonso, L., Celesti, M., Cogliati, S., Colombo, R., Damm, A., Douglas, S., Guanter, L., Hanuš, J., Kataja, K., Kraska, T., Matveeva, M., Moreno, J., Muller, O., Pikl, M., Pinto, F., Quiros Vargas, J., Rademske, P., Rodriguez-Morene, F., Sabater, N., Schikling, A., Schüttemeyer, D., Zemek, F., Rascher, U., 2019. The high-performance airborne imaging spectrometer hyplant–from raw images to top-of-canopy reflectance and fluorescence products: introduction of an automatized processing chain. Remote Sens. 11 (2760), http://dx.doi.org/10.3390/rs11232760.

Soltani, M., Mauder, M., Laux, P., Kunstmann, H., 2018. Turbulent flux variability and energy balance closure in the TERENO prealpine observatory: A hydrometeorological data analysis. Theor. Appl. Climatol. 133, 937–956. http://dx.doi.org/10.1007/s00704-017-2235-1.

Taylor, K.E., Stouffer, R.J., Meehl, G.A., 2012. An overview of CMIP5 and the experiment design. Bull. Am. Meterol. Soc. 93, 485–498. http://dx.doi.org/10.1175/BAMS-D-11-00094.1.

Udina, M., Peinó, E., Polls, F., Mercader, J., Guerrero, I., Valmassoi, A., Paci, A., Bech, J., 2024. Irrigation impact on boundary layer and precipitation characteristics in WRF model simulations during LIAISE-2021. Q. J. R. Meteorol. Soc. http://dx.doi.org/10.1002/qj.4756.

Van Kesteren, B., Hartogensis, O., van Dinther, D., Moene, A.F., De Bruin, H.A.R., 2013. Measuring of H_2O and CO_2 fluxes at field scales with scintillometry: Part I - Introduction and validation of four methods. Agric. Forest Meteorol. 178–179, 75–87. http://dx.doi.org/10.1016/j.agrformet.2012.09.013.

van Leeuwen, C., Giovanni, G.S., Bois, B., Ollat, N., Swingedouw, D., Zito, S., Gambetta, G.A., 2024. Climate change impacts and adaptations of wine production. Nat. Rev. Earth Environ. 5, 258–275. http://dx.doi.org/10.1038/s43017-024-00521-5.

Vicente-Serrano, S.M., Zabalza-Martínez, J., Borràs, G., López-Moreno, J.I., Pla, E., Pascual, D., Savé, R., Biel, C., Funes, I., Martín-Hernández, N., Peña-Gallardo, M., 2017. Effect of reservoirs on streamflow and river regimes in a heavily regulated river basin of northeast Spain. Catena 149, 727–741. http://dx.doi.org/10.1016/j.catena.2016.03.042.

Vickers, D., Mahrt, L., 1997. Quality control and flux sampling problems for tower and aircraft data. J. Atmos. Ocean. Tech. 14, 512–526. http://dx.doi.org/10.1175/1520-0426(1997)014<0512:QCAFSP>2.0.CO;2.

Wang, C., Tian, W., Parker, D.J., Marsham, J.H., Guo, Z., 2011. Properties of a simulated convective boundary layer over inhomogeneous vegetation. Q. J. R. Meteorl. Soc. 137, 99–117. http://dx.doi.org/10.1002/qj.724.

Ward, H.C., Evans, J.G., Hartogensis, O.K., Moene, A.F., De Bruin, H.A.R., Grimmond, C.S.B., 2013. A critical revision of the estimation of the latent heat flux from two-wavelength scintillometry. Q. J. R. Meteorol. Soc. 139, 1912–1922. http://dx.doi.org/10.1002/qj.2076.

Webb, E.K., Pearman, G.I., Leuning, R., 1980. Correction of flux measurements for density effects due to heat and water vapor transfer. Q. J. R. Meteorol. Soc. 106, 85–100. http://dx.doi.org/10.1002/qj.49710644707.

Wilczak, J.M., Oncley, S.P., Stage, S.A., 2001. Sonic anemometer tilt correction algorithms. Bound.-Layer Meteorol. 99, 127–150. http://dx.doi.org/10.1023/A:1018966204465.

Wrenger, B., Cuxart, J., 2024. Vertical profiles of temperature, wind and turbulent fluxes across a deciduous forest over a slope observed with an UAV. Front. Earth Sci.-Atmos. Sci. 19, http://dx.doi.org/10.3389/feart.2024.1159679.

Zribi, M., Dehaye, V., Dassas, K., Fanise, P., Le Page, M., Laluet, P., Boone, A., 2022. Airborne GNSS-R polarimetric multi-incidence data analysis for soil moisture surface estimation over an agricultural site. IEEE J. Sel. Top. Appl. Earth Obs. Remote. Sens. 15, 8432–8441. http://dx.doi.org/10.1109/JSTARS.2022.3208838.